HHS Public Access

Author manuscript

Inorg Chem. Author manuscript; available in PMC 2017 September 06.

Published in final edited form as:

Inorg Chem. 2016 September 06; 55(17): 8646–8660. doi:10.1021/acs.inorgchem.6b01219.

The Influence of Peripheral Substituent Modification on P^{V}, Mn^{III}, and $Mn^{V}(O)$ Corrolazines: X-ray Crystallography, Electrochemical and Spectroscopic Properties, and HAT and OAT Reactivities

Evan E. Joslin[†], **Jan Paulo T. Zaragoza**, **Regina A. Baglia**, **Maxime A. Siegler**, and **David P. Goldberg**[*]

Department of Chemistry, The Johns Hopkins University, 3400 North Charles Street, Baltimore, Maryland 21218, United States

Abstract

The influence of remote peripheral substitution on the physicochemical properties and reactivity of phosphorus and manganese corrolazine (Cz) complexes was examined. The substitution of *p*-MeO for *p*-*t*-Bu groups on the eight phenyl substituents of the *β*-carbon atoms of the Cz ring led to changes in UV–vis transitions and redox potentials for each of the complexes. The oxygen atom transfer (OAT) and hydrogen atom transfer (HAT) reactivity of the $Mn^{V}(O)$ complexes was also influenced by *p*-MeO substitution. The OAT reactivity of $Mn^{V}(O)(MeOP_8Cz)$ ($MeOP_8Cz$ = octakis-(*p*-methoxyphenyl)corrolazinato^{3-}) with triarylphosphine (PAr_3) substrates led to second-order rate constants from 10.2(5) to 3.1(2) × 10^4 M^{-1} s^{-1}. These rates of OAT are slower than those seen for $Mn^{V}(O)(TBP_8Cz)$ (TBP_8Cz = octakis(*p*-*tert*-butylphenyl) corrolazinato^{3-}). A Hammett study involving *para*-substituted PAr_3 substrates reveals a Hammett *ρ*-value for $Mn^{V}(O)(MeOP_8Cz)$ that is more negative than that observed for $Mn^{V}(O)(TBP_8Cz)$, consistent with a less electrophilic Mn center. The HAT reactivity of $Mn^{V}(O)(MeOP_8Cz)$ with C–H substrates was examined and revealed second-order rate constants from 6.8(5) × 10^{-5} to 1.70(2) × 10^{-1} M^{-1} s^{-1}. The rate constants varied with the C–H bond strength of the substrate. Slightly faster HAT rates with C–H substrates were observed with $Mn^{V}(O)(MeOP_8Cz)$ compared to $Mn^{V}(O)(TBP_8Cz)$, indicating that the basicity of the putative $[Mn^{IV}(O)]^{-}$ intermediate likely compensates for the more negative redox potential in the driving force for HAT. In addition, the complete, large-scale synthesis of the *para*-phenyl-substituted porphyrazines RP_8PzH_2 (R = *p*-*tert*-butylphenyl (TB), *p*-methoxyphenyl (MeO), and *p*-isopropylphenyl) and corrolazines RP_8CzH_3 (TBP_8CzH_3 and

[*]Corresponding Author: dgp@jhu.edu.

[†]**Present Address**

Faculty at Sewanee: The University of the South; 735 University Avenue, Sewanee, Tennessee 37383, United States

The authors declare no competing financial interest.

Supporting Information The Supporting Information is available free of charge on the ACS Publications website at DOI: 10.1021/acs.inorgchem. 6b01219.

UV–vis absorption spectral data, illustrated bond lengths in macrocyclic core, electron density difference Fourier maps, NMR spectra, cyclic voltammogram, product analysis, kinetics analyses (PDF)

X-ray crystallographic data (CIF)

X-ray crystallographic data (CIF)

X-ray crystallographic data (CIF)

$MeOP_8CzH_3$) is presented. The crystal structures of the monoprotonated, metal-free corrolazine $[(TBP_8CzH_3)(H)]^+[BArF]^-$, $P^V(OMe)_2$-($MeOP_8Cz$), and $Mn^{III}(MeOP_8Cz)(MeOH)$ are presented. This work provides the first insights into the influence of electronic substituent effects on the corrolazine periphery.

Graphical abstract

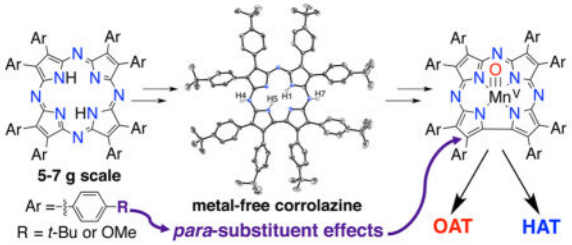

INTRODUCTION

Over a decade ago, our lab published the first examples of ring-contracted porphyrazines, which we named corrolazines in analogy with both porphyrazines and corroles.[1] We envisioned that these porphyrinoid ligands would provide access to a variety of new metal complexes and exhibit novel spectroscopic features and reactivity that would be quite distinct from porphyrins, porphyrazines, and corroles. One anticipated property of particular interest to us was the stabilization of high oxidation states at the central metal, which was also seen in the analogous corrole[2–10] complexes. This property would allow us to target species that mimic reactive intermediates in both heme enzymes and synthetic catalysts, including highvalent metal-oxo species analogous to Compound-I (Fe^{IV}(O)-(porph$^{\bullet+}$)) and Compound-II (Fe^{IV}(O)(porph)) in the Cytochrome P450s, peroxidases, and catalases.[11–17] We hypothesized that the corrolazine ligand would also be useful in new metalloporphyrinoid catalysts, especially for reactions involving the oxidation of organic substrates. The inclusion of nitrogen atoms at the *meso* positions was expected to afford enhanced reactivity of high-valent species based on simple electronegativity arguments, while also adding stability to the macrocyclic ring. Following the initial synthesis of the first corrolazine, it has been shown that the corrolazine ligand does stabilize a number of high-valent metal complexes, including copper(III), vanadium(V),[18] cobalt(IV),[19] iron(IV),[20,21] iron-(III),[22] rhenium(V),[23] chromium(V),[24] and an isolable manganese(V)-oxo complex[25] (Figure 1). The Mn^V(O) complex exhibited oxidative reactivity in oxygen atom transfer (OAT) and hydrogen atom transfer (HAT) reactions, and this complex provided a means to study the influence on reactivity of a range of biomimetic modifications, including the addition of axial ligands,[26–28] and the addition of protons and Lewis acids.[29–32] However, the effect of modifying the peripheral substituents on the β-carbon atoms of the corrolazine ring was not examined.

The variation of the substituents on the *meso* and β-positions of porphyrins has been well-studied for their influence over the properties of both the internal metal and the macrocyclic ring.[33–36] The spectroscopic effects of varying the substituents on the β-positions of porphyrazines,[37,38] phthalocyanines,[39] tetrapyrazinocorrolazines,[40] and

triazatetrabenzcorroles[41–43] has also been examined. These kinds of substitutions were made as part of a wide range of efforts, including the development of new dye-sensitized solar cells (DSSCs)[44–46] and the synthesis of molecules for photodynamic therapy (PDT).[34] In addition, varying the substituents at the peripheral positions allowed for the study of their influence on a wide range of metal-mediated reactions, including the oxidation of organic substrates.

Herein we describe the influence of remote substitution at the peripheral *β*-carbon substituents on the spectroscopic properties, redox potentials, and reactivity of phosphorus and manganese corrolazines. The remote *p*-*t*-Bu groups on the eight peripheral phenyl rings were substituted with *p*-MeO groups. The HAT and OAT reactivity of $Mn^{V}(O)$ complexes for the *p*-MeO and *p*-*t*-Bu derivatives was examined. Even though the *para* substituents on the *β*-carbon aryl rings are remote from the metal center, it was found that they still exert a significant influence on the spectroscopic and reactivity properties of these porphyrinoid compounds. The complete synthesis of the peripherally substituted, metal-free corrolazine ligands TBP_8CzH_3 (TBP_8Cz = octakis(*p*-*tert*-butylphenyl)-corrolazinato^{3-}) and $MeOP_8CzH_3$ ($MeOP_8Cz$ = octakis(*p*methoxyphenyl) corrolazinato^{3-}; Figure 1) is also presented. The synthesis of the TBP derivative was described in brief in an earlier report,[47] but in this work we present the improved, large-scale synthesis of this compound from commercially available starting materials in one practical report. The same synthetic strategy was used to prepare the *para*-methoxy derivative, and these syntheses are described in sufficient detail so as to make it easy for other laboratories to prepare the corrolazine ligand. During the course of this work, new porphyrazines ($MeOP_8PzH_2$, iPr_8PzH_2) were also synthesized, as well as the new P^{V}, Mn^{III}, and $Mn^{V}(O)$ corrolazines (Figure 1).

EXPERIMENTAL SECTION

General Procedures

All reactions were performed using dry solvents and standard Schlenk techniques unless otherwise noted. Dichloromethane, tetrahydrofuran (THF), diethyl ether, and methanol were purified via a Pure-Solv solvent purification system from Innovative Technologies. Dichloromethane-d_2 and chloroform-d_1 were obtained from Cambridge Isotopes, Inc. The synthesis of 9,10-dihydro-10-methylacridine ($AcrH_2$),[49] $[H(OEt_2)_2][B\{C_6H_3(m\text{-}CF_3)_2\}_4]$ (HBArF),[50] $Mn^{III}(TBP_8Cz)$, and $Mn^{V}(O)(TBP_8Cz)$[47] followed literature procedures. Xanthene (Xn) was obtained from commercial sources and purified by recrystallization with ethanol, and 1,4-cyclohexadiene was filtered through neutral alumina prior to kinetics experiments. All other reagents were purchased from commercial sources and used without further purification.

Instrumentation

^{1}H NMR spectra were recorded on a Bruker 300 MHz or a Bruker Avance 400 MHz spectrometer. ^{13}C NMR spectra were recorded on a Bruker 300 MHz or a Bruker 400 MHz spectrometer (operating frequency 101 or 151 MHz, respectively). All ^{1}H and ^{13}C NMR spectra are referenced against residual proton signals (^{1}H NMR) or the ^{13}C resonances of the deuterated solvent (^{13}C NMR). ^{31}P NMR spectra were obtained on a Bruker 400 MHz

(operating frequency 161.9 MHz) spectrometer and referenced against an external standard of H_3PO_4 ($\delta = 0$). Elemental analyses were performed at Atlantic Microlab, Inc, in Norcross, GA. Electrochemical experiments were performed under an argon atmosphere using a BAS 100B electrochemical analyzer. Cyclic voltammograms were recorded in CH_2Cl_2 using a standard three-electrode cell with a glassy carbon working electrode and tetrabutylammonium hexafluorophosphate ($TBAPF_6$, 0.1 M) as electrolyte unless otherwise noted. All potentials are reported versus Fc^+/Fc. UV–vis measurements were performed on a Hewlett-Packard 8453 diode-array spectrophotometer with a 3.5 mL air-free quartz cuvette (path length = 1 cm) fitted with a glass stopper or rubber septum. A 400 nm long-pass filter was employed to prevent photo-decomposition by placing the filter directly between the sample quartz cuvette and the spectrophometer light source. For reactions with total reaction time of less than 10 s, stopped-flow experiments were performed using HiTech SHU-61SX2 (TgK Scientific Ltd.) with a xenon light source and Kinetic Studio software. Laser desorption/ionization mass spectrometry (LDI-MS) was collected on a Bruker Autoflex III/TOF/TOF instrument equipped with a nitrogen laser at 335 nm using an MTP 384 ground steel target plate.

Single Crystal X-ray Crystallography

Reflection intensities were measured at 110(2) K for $P^V(MeOP_8Cz)(OMe)_2$ and $[(TBP_8CzH_3)(H)]^+[BArF]^-$ or 93(2) K for $Mn^{III}(MeOP_8Cz)$-(HOMe) using a SuperNova diffractometer (equipped with Atlas detector) with Cu Kα radiation (λ = 1.541 78 Å) under the program CrysAlisPro (Version 1.171.36.32 Agilent Technologies, 2013). The same program was used to refine the cell dimensions and for data reduction. The structure was solved with the program SHELXS-2013 and was refined on F^2 with SHELXL-2013.[51] Analytical numeric absorption correction based on a multifaceted crystal model was applied using CrysAlisPro. The temperature of the data collection was controlled using the system Cryojet (manufactured by Oxford Instruments). The H atoms were placed at calculated positions using the instructions AFIX 43 or AFIX 137 with isotropic displacement parameters having values 1.2 or 1.5 U_{eq} of the attached C atoms.

$[(TBP_8CzH_3)(H)]^+[BArF]^-\cdot$4.18 Toluene Crystallographic Data—The positions of the H atoms attached to N3, N4, N6, and N7 were unambiguously determined by reconstructing the contoured difference Fourier maps within the plane defined by the three neighboring C–N–C atoms (e.g., C5–N3–C8 for the H atom attached to N3). The structure of $[(TBP_8CzH_3)(H)]^+[BArF]^-$ is partly disordered. For the corrolazine, two *t*-butyl groups (the six others are ordered) were found to be disordered over two orientations, and the occupancy factors of the major components of the disorder refine to 0.588(7) and 0.683(4). The BArF counterion is also disordered, as three $-CF_3$ groups can be found in two different orientations. The occupancy factors of the major components of the disorder refine to 0.723(10), 0.663(9), and 0.787(5). The crystal lattice contains some solvent molecules. There are five (but not all are fully occupied) toluene molecules in the asymmetric unit, and their occupancy factors were either refined freely or were fixed. Three of those molecules are treated as ordered, and their occupancy factors refine to 0.977(4), 0.909(4), and 0.793(4). A fourth solvent molecule (fully occupied) is disordered over two orientations, and the occupancy factor of the major component refines to 0.823(4). A fifth solvent molecule is

found at sites of inversion symmetry, and consequently the occupancy factor must be constrained to 0.5 by symmetry. Overall, the ratio of corrolazine/BArF/toluene in the crystal is 1:1:4.18.

Data for $[(TBP_8CzH_3)(H)]^+[BArF]^-$ follow: Fw = 2608.10, dark brown block, 0.45 × 0.24 × 0.12 mm^3, triclinic, $P\bar{1}$ (No. 2), a = 16.2718(3), b = 19.8352(3), c = 23.4803(3) Å, α = 99.8050(11), β = 109.3816(13), γ = 91.7165(12)°, V = 7013.9(2) Å3, Z = 2, D_x = 1.235 g cm^{-3}, μ = 0.782 mm^{-1}, T_{min}–T_{max}: 0.796–0.927. 93 671 Reflections were measured up to a resolution of (sin θ/λ_{max}) = 0.62 $Å^{-1}$. 27 531 Reflections were unique (R_{int} = 0.0249), of which 23 693 were observed [$I > 2\sigma(I)$]. 1999 Parameters were refined using 1005 restraints. $R1/wR2$ [$I > 2\sigma(I)$]: 0.0586/0.1689. $R1/wR2$ [all refl]: 0.0664/0.1779. S = 1.025. Residual electron density found between −0.58 and 0.78 e $Å^{-3}$.

$P^V(MeOP_8Cz)(OMe)_2$ Crystallographic Data—The structure for $P^V(MeOP_8Cz)(OMe)_2$ is partly disordered. The methoxyphenyl groups C17→C23, C24→C30, and C31→C37 are found to be disordered over either two or three orientations, and the occupancy factors of the major components of the disorder refine to 0.653(7), 0.803(5), and 0.526(3), respectively. The crystal lattice contains some very disordered solvent molecules (CH_2Cl_2), and their contribution was taken out in the final refinement (SQUEEZE details are provided in the CIF file).[52]

Data for $P^V(MeOP_8Cz)(OMe)_2$: Fw = 1240.27, dark lath, 0.45 × 0.05 × 0.03 mm^3, triclinic, $P\bar{1}$ (No. 2), a = 14.8549(6), b = 15.6119(18), c = 16.6521(7), α = 87.211(4), β = 66.674(4), γ = 74.628(4)°, V = 3412.4(5) $Å^3$, Z = 2, D_x = 1.207 g cm^{-3}, μ = 0.869 mm^{-1}, T_{min}–T_{max}: 0.822–0.977. 43 404 Reflections were measured up to a resolution of $(\sin \theta/\lambda)_{max}$ = 0.62 $Å^{-1}$. 13 452 Reflections were unique (R_{int} = 0.0635), of which 9906 were observed [$I > 2\sigma(I)$]. 1103 Parameters were refined using 1150 restraints. $R1/wR2$ [$I > 2\sigma(I)$]: 0.0573/0.1466. $R1/wR2$ [all refl]: 0.0798/0.1623. S = 1.014. Residual electron density found between −0.38 and 0.76 e $Å^{-3}$.

$Mn^{III}(MeOP_8Cz)(HOMe)\cdot 0.9CHCl_3\cdot 1.39MeOH$ Crystallographic Data—The H atoms from the MeOH molecules could not be successfully retrieved. The structure is partly disordered. The methoxyphenyl group C24→C30 and coordinated methanol molecule are found to be disordered over two orientations, and the occupancy factors of the major components of the disorder refine to 0.765(12) and 0.742(10). The crystal lattice contains some amount of lattice solvent molecules (ordered MeOH and disordered $CHCl_3$). The B level alert suggests one unusually short H···H contact. H74C belongs to one partially occupied (occupancy factor: 0.607(10)) lattice MeOH solvent molecule. Thus, it is very difficult to determine accurately the positions of the H atoms attached to C74 from X-ray data, and C74 was treated as an idealized CH_3 group using the AFIX 137 instruction. Most likely, the positions of those H atoms which are slightly different. The occupancy factors for all lattice solvent molecules were refined freely, and there is ca. 0.9 × $CHCl_3$ and 1.39 × MeOH in the asymmetric unit.

Data for $Mn^{III}(MeOP_8Cz)(HOMe)$: Fw = 1383.77, thin dark brown plate, 0.61 × 0.24 × 0.02 mm^3, triclinic, $P\bar{1}$ (No. 2), a = 10.0064(5), b = 18.3946(9), c = 19.5794(9), α = 69.721(4), β

= 86.165(4), γ = 80.387(4)°, V = 3332.9(3) Å^3, Z = 2, D_x = 1.379 g cm^{-3}, μ = 3.158 mm^{-1}, T_{min}–T_{max}: 0.349–0.936. 42 229 Reflections were measured up to a resolution of (sin $\theta/\lambda)_{max}$ = 0.62 Å^{-1}. 12 960 Reflections were unique (R_{int} = 0.0574), of which 9476 were observed [$I > 2\sigma(I)$]. 1006 Parameters were refined using 382 restraints. $R1/wR2$ [$I > 2\sigma(I)$]: 0.0695/0.1949. $R1/wR2$ [all refl]: 0.0920/0.2181. S = 1.042. Residual electron density found between −0.75 and 1.21 e Å^{-3}.

Bis(4-methoxyphenyl)fumaronitrile—The synthesis of bis(4-methoxyphenyl)fumaronitrile was previously reported by an alternative procedure, and all characterization data match the reported literature values.[53] An amount of (4-methoxyphenyl)acetonitrile (10.0 g, 0.0679 mol) and I_2 (17.2 g, 0.0679 mol) was dissolved in 35 mL of Et_2O. NaOMe in MeOH (55 mL, 3.1 M) was slowly added by an addition funnel to the stirring solution at −78 °C. The reaction was allowed to stir at −78 °C for 1.5 h, and at 0 °C for an additional 2 h. The dark red solution slowly changed to yellow, and a precipitate formed. The yellow solid was collected by filtration through a Büchner funnel, washed with 1:1 MeOH/H_2O, and dried under vacuum to yield a bright yellow solid (5.98 g, 61%).

Bis(4-*tert*-butylphenyl)fumaronitrile—The synthesis of bis(4-*tert*-butylphenyl)fumaronitrile was previously reported by an alternative procedure, and all characterization data match the reported literature values.[48,54] An amount of (4-*tert*-butylphenyl)acetonitrile (20.6 g, 0.119 mol) and I_2 (30.3 g, 0.119 mol) was dissolved in 500 mL of Et_2O. NaOMe in MeOH (3.04 M, 100 mL) was slowly added by an addition funnel to the stirring solution at 0 °C. The dark red solution slowly changed to yellow, and a precipitate formed. The white solid was collected via filtration through a Büchner funnel and washed with MeOH and dried under vacuum. A second batch of product could be isolated after concentration of the filtrate by approximately half and then placing in a freezer (−20 °C) for 12 h. The second batch was isolated in the same way as the first batch to yield a white solid (15.3 g, 75% yield).

Bis(4-isopropylphenyl)fumaronitrile—An amount of (4-isopropylphenyl)acetonitrile (10 g, 0.063 mol) and I_2 (16 g, 0.063 mol) was dissolved in 250 mL of Et_2O. NaOMe in MeOH (80 mL, 1.6 M) was slowly added by an addition funnel to the stirring solution at 0 °C. The reaction was stirred at −78 °C, and a solid immediately precipitated out. The white solid was collected by filtration through a Büchner funnel, washed with MeOH, and dried under vacuum to yield a white solid. A second batch of product could be isolated by placing the filtrate in the freezer for 12 h (7.3 g, 74%). ^{1}H NMR (400 MHz, $CDCl_3$) δ 7.77 (d, $^3J_{HH}$ = 8 Hz, 4H, Ar-*H*), 7.38 (d, $^3J_{HH}$ = 8 Hz, 4H, Ar-*H*), 2.99 (hept, $^3J_{HH}$ = 7 Hz, 2H, C*H*(CH_3)$_2$), 1.29 (d, $^3J_{HH}$ = 7 Hz, 12H, CH(C*H*$_3$)$_2$). ^{13}C NMR (101 MHz, $CDCl_3$) δ 153.15, 129.79, 128.89, 127.46 (Ar-*C*), 124.61 (alkene-*C*), 117.19 (*C*N), 34.29 (*C*H(CH_3)$_2$), 23.80 (CH(*C*H_3)$_2$).

3,4-Bis(2-methoxy)pyrroline-2,5-diimine—Bis(4-methoxyphenyl)fumaronitrile (5.01 g, 0.0173 mol) was placed in 330 mL of ethylene glycol and heated to 115 °C. An amount of sodium metal (0.0530 g, 0.00268 mol) was added to the heterogeneous refluxing solution.

Ammonia gas was rapidly bubbled through the solution for 1.25 h, and the reaction mixture turned a dark blue and became homogeneous. The solution was filtered hot through a Büchner funnel to remove any unreacted starting material. The filtrate was added to ice water to induce precipitation and allowed to sit for 45 min. The solid was collected on a Büchner funnel and washed with copious amounts of water. The solid was left to dry for 12 h under vacuum to yield a light yellow solid (3.90 g, 73% yield).

3,4-Bis(2-*tert*-butylphenyl)pyrroline-2,5-diimine—The compound was synthesized via the same procedure as 3,4-bis(2-methoxy)pyrroline-2,5-diimine starting with bis(4-*tert*-butylphenyl)-fumaronitrile (4.72 g, 0.0138 mol). The product was isolated as a pale yellow solid (2.55 g, 51% yield). All characterization data match the literature values.[48,54]

2,3,7,8,12,13,17,18-Octakis(4-methoxyphenyl) porphyrazine ($MeOP_8PzH_2$)

Route 1: $MeOP_8PzMg$ was synthesized previously via an alternative procedure.[37] Magnesium metal (0.0446 g, 1.85 mmol) and a small chip of I_2 were refluxed in *n*-BuOH (10 mL) under argon until all the Mg metal had been consumed (~2 h), yielding a white suspension. An amount of 3,4-bis(2-methoxy)pyrroline-2,5-diimine (1.41 g, 4.60 mmol) was added, and the reaction mixture was refluxed for 12 h. The solution immediately turned dark yellow and then slowly converted to a dark green-blue. The *n*-BuOH was removed under vacuum, and the residue was dissolved in CH_2Cl_2 (60 mL). Excess CF_3CO_2H (TFA; 14 mL) was added, and the reaction mixture turned from dark green-blue to a dark blue. The reaction mixture was stirred in the dark for 12 h, the CH_2Cl_2 was removed by a stream of air, and the remaining blue slurry was poured over ice water (200 mL) and neutralized with concentrated ammonium hydroxide. The solid was collected by filtration and washed thoroughly with water and MeOH and then dried under vacuum to yield $MeOP_8PzH_2$ as dark purple solid (0.984 g, 53%).

Route 2: Magnesium metal (0.367 g, 0.0151 mol) was added to 30 mL of a 5:1 1-octanol/1-pentanol solution. The reaction mixture was refluxed until all the metal had reacted, yielding a viscous gray suspension. Bis(4-methoxyphenyl)fumaronitrile (4.00 g, 0.0138 mol) was added to the reaction mixture and allowed to reflux for 12 h. The reaction mixture turned dark brown-purple. The reaction mixture was poured into ~500 mL of MeOH to induce precipitation and filtered through a Büchner funnel, and the solid was washed with copious amounts of methanol until the filtrate was colorless. The blue-green solid was washed with pentane and dried under vacuum (2.60 g, 65% yield). ^{1}H NMR, UV–vis, and LDI-MS matched previously reported data for $Mg^{II}(MeOP_8Pz)$.[37]

$Mg^{II}(MeOP_8Pz)$ (2.60 g, 0.002 19 mol) was dissolved in CH_2Cl_2 (50 mL) and excess TFA (20 mL). The solution instantly turned to a dark blue and was left to stir in the dark for 3 h. The CH_2Cl_2 was evaporated, and the blue solution was poured into 400 mL of ice water and neutralized with NH_4OH. The reaction mixture was filtered through a Büchner funnel and washed with copious amounts of MeOH. The solid was dried under vacuum to yield a dark purple solid (1.41 g, 55%). Well-resolved NMR spectroscopic data could not be obtained because $MeOP_8PzH_2$ is poorly soluble in common solvents. UV–vis (pyridine) λ_{max} [nm]

381, 522, 636, 692, 719. Anal. Calcd for $C_{72}H_{58}N_8O_8$: C, 74.34; H, 4.63; N, 8.05. Found: C, 73.99; H, 5.03; N, 9.63%. LDI-MS [M^+] m/z = 1163.34 Calcd for $C_{72}H_{58}N_8O_8$ 1163.30.

2,3,7,8,12,13,17,18-Octakis(4-*tert*-butylphenyl) porphyrazine (TBP_8PzH_2)

Route 1: TBP_8PzH_2 was synthesized previously via an alternative procedure.[37,47,55,56] Magnesium metal (0.0420 g, 1.72 mmol) and a small chip of I_2 were refluxed in *n*-BuOH (12 mL) until all the Mg metal had been consumed, yielding a white suspension. An amount of 3,4-bis(2-*tert*-butylphenyl)pyrroline-2,5-diimine (2.00 g, 5.84 mmol) was added to the reaction mixture, and the reaction immediately turned dark yellow and then slowly converted to a dark green-blue. The reaction was refluxed for 24 h. The *n*-BuOH was removed under vacuum, and the residue was dissolved in excess TFA (15 mL) and stirred in the dark for 12 h. The reaction mixture was poured over ice water and neutralized with concentrated NH_4OH. The solid was collected by filtration, washed thoroughly with water and MeOH, and dried under vacuum to yield a dark green solid (1.20 g, 63%).

Route 2: Magnesium metal (0.594 g, 0.0245 mol) was added to 53 mL of a 5:1 1-octanol/1-pentanol solution. The reaction mixture was refluxed until all the metal reacted, yielding a viscous gray suspension. An amount of bis(4-*tert*-butylphenyl)fumaronitrile (8.21 g, 0.0240 mol) was added, and the reaction mixture was refluxed for 3 h. The solvent was removed via vacuum distillation, and the residual solid was washed with H_2O, collected on a Büchner funnel, washed with MeOH and pentane, and dried under vacuum to give $Mg^{II}(TBP_8Pz)$ as a blue-green solid (6.88 g, 83% yield). UV–vis and LDI-MS matched previously reported data for $Mg^{II}(TBP_8Pz)$.[37,57]

An amount of $Mg^{II}(TBP_8Pz)$ (6.88 g, 0.00492 mol) was dissolved in CH_2Cl_2 (20 mL) and TFA (30 mL) and stirred for 3 h, in which time the solution turned dark blue. CH_2Cl_2 was removed by evaporation under a stream of air. The reaction mixture was poured into ice water, neutralized with NH_4OH, and filtered through a Büchner funnel. The solid was washed with copious amounts of water and MeOH and dried under vacuum to yield a dark green solid (3.50 g, 52%).

2,3,7,8,12,13,17,18-Octakis(4-isopropylphenyl) porphyrazine ($iPrP_8PzH_2$)—

Magnesium metal (0.153 g, 0.00637 mol) was added to 13 mL of a 5:1 1-octanol/1-pentanol solution. The reaction mixture was refluxed until all the metal had reacted, yielding a viscous gray suspension. Bis(4-isopropylphenyl)fumaronitrile (2.00 g, 0.00636 mol) was added, and the reaction mixture was refluxed for 2 h, in which time the solution turned dark green-blue. The solvent was removed via vacuum distillation to yield a blue-green solid (UV–vis (CH_2Cl_2) λ_{max} [nm] 379, 640; LDI-MS [M^+] m/z = 1281.97 calcd for $C_{88}H_{88}N_8Mg$ 1282.30). The solid was dissolved in CH_2Cl_2 (20 mL) and TFA (10 mL), and the solution immediately turned to a dark blue and was left to stir in the dark for 12 h. The CH_2Cl_2 was evaporated, and the blue solution was poured on ice and neutralized with NH_4OH. The reaction mixture was filtered through a Büchner funnel and washed with copious amounts of MeOH. The solid was dried under vacuum to yield a dark blue-green solid. (1.6 g, 82%). Well-resolved NMR spectroscopic data could not be obtained because

iPrP_8PzH_2 is poorly soluble in common solvents. UV–vis (CH_2Cl_2) λ_{max} [nm] 371, 454, 604, 670. LDI-MS $[M]^+$ m/z = 1259.74 calcd for $C_{88}H_{90}N_8$ 1259.74.

[P^V(MeOP_8Cz)(OH)][OH]—MeOP_8PzH_2 (1.09 g, 0.869 mmol) was dissolved in pyridine (200 mL) and heated to reflux and then PBr_3 (1.8 mL, 19 mmol) was added by syringe directly into the refluxing reaction. The reaction was refluxed 12 h, in which time the solution turned from dark green to dark red. An additional 30 equiv of PBr_3 (2.8 mL, 30 mmol) was added, the reaction was refluxed for an additional 6 h, then a final addition of 30 equiv of PBr_3 (2.8 mL, 30 mmol) was added, and the reaction mixture was refluxed for 12 h. The reaction mixture was cooled to room temperature, methanol was added via syringe to quench the reaction, and the solution became dark green. The reaction mixture was reduced under vacuum to dryness; the remaining dark brown-green solid was dissolved in CH_2Cl_2 and filtered through a silica plug, and the plug was washed with 8:2 CH_2Cl_2/EtOAc. A small amount of solid silica was added to the filtrate and this mixture was reduced to dryness. The product fused on silica was purified on a silica gel column with 8:2 CH_2Cl_2/EtOAc (R_f = 0.82). The solid was collected, washed with CH_3CN, and dried under vacuum to yield a dark green solid (0.555 g, 49%). ^{1}H NMR (300 MHz, CD_2Cl_2) δ 8.37–8.24 (m, 8H, Ar-*H*), 8.13 (d, $^3J_{HH}$ = 8.8 Hz, 4H, Ar-*H*), 7.26–7.17 (m, 8H, Ar-*H*), 7.10 (d, $^3J_{HH}$ = 8.9 Hz, 4H, Ar-*H*), 7.04 (vb s, 4H, Ar-*H*), 6.68 (d, $^3J_{HH}$ = 8.3 Hz, 4H, Ar-*H*), 4.00 (s, 6H, Ar-OCH_3), 3.99 (s, 6H, Ar-OCH_3), 3.94 (s, 6H, Ar-OCH_3), 3.91 (s, 6H, Ar-OCH_3). ^{13}C NMR (101 MHz, $CDCl_3$) δ 160.00, 159.88, 159.61, 146. 01, 144.85, 142.33, 139.13, 136.10, 134.55, 134.42, 134.08, 132.33, 126.08, 125.77, 114.06, 113.90 (all s, all related to Ar-carbons, eight aryl-carbon signals missing due to coincidental overlap), 55.56 (s, Ar–O*C*H_3), 55.49 (s, Ar–O*C*H_3), 55.07 (s, Ar–O*C*H_3), one methoxy carbon signal missing due to coincidental overlap. ^{31}P NMR (162 MHz, $CDCl_3$) δ −111.35. Cyclic voltammetry (CV; CH_2Cl_2, 50 mV): $E_{1/2}$ = 0.65 V, $E_{1/2}$ = −1.27 V, $E_{1/2}$ = −1.78 V. UV–vis (CH_2Cl_2) λ_{max} [nm] ($\varepsilon \times 10^{-4}$ M^{-1} cm^{-1}) 461 (8.2), 557 (0.96), 594 (1.2), 644 (4.5). Anal. Calcd for $C_{72}H_{58}N_7O_{10}P$: C, 71.34; H, 4.82; N, 8.09. Found: C, 71.13; H, 4.98; N, 7.94%. LDI-MS m/z = $[M – OH]^+$ 1194.73 calcd for $C_{72}H_{57}N_7O_9P$ 1193.39.

P^V(MeOP_8Cz)(OMe)$_2$—Crystals of P^V(MeOP_8Cz)(OMe)$_2$ were obtained via slow diffusion of MeOH into a CH_2Cl_2 solution of [P^V(MeOP_8Cz)(OH)][OH]. The sample was allowed to sit in the dark for ~2 d. The solid was collected on a Büchner funnel, washed with MeOH and hexanes, and allowed to dry under vacuum yielding a dark purple solid. ^{1}H NMR (400 MHz, benzene-d_6) δ 8.71 (d, $^3J_{HH}$ = 8.8 Hz, 3H, Ar-*H*), 8.66 (d, $^3J_{HH}$ = 8.8 Hz, 3H, Ar-*H*), 8.58 (d, $^3J_{HH}$ = 8.8 Hz, 3H, Ar-*H*), 7.48 (d, $^3J_{HH}$ = 8.5 Hz, 4H, Ar-*H*), 7.12 (s, 2H, Ar-*H*), 7.05 (d, $^3J_{HH}$ = 8.9 Hz, 3H, Ar-*H*), 6.59–6.54 (m, 4H, Ar-*H*), 3.47 (two s, 12H, each a Ar-OCH_3), 3.43 (s, 6H, Ar-OCH_3), 3.37 (s, 6H, Ar-OCH_3), −1.69 (d, $^3J_{HP}$ = 21.9 Hz, 6H, axial-OCH_3). ^{31}P NMR (162 MHz, C_6DC_6) δ −192.7. UV–vis (CH_2Cl_2) λ_{max} [nm] 451, 594, 644. LDI-MS m/z = $[M – OMe]^+$ 1208.69 calcd for $C_{73}H_{59}N_7O_9P$ 1208.41.

[P^V(TBP$_8$Cz)(OH)]OH—Two reactions were run simultaneously and combined prior to purification. To a refluxing solution of compound TBP$_8PzH_2$ (1.20 g, 0.875 mmol and 0.900 g, 0.656 mmol) in pyridine (250 mL) was added PBr_3 (2.85 and 2.14 mL, 35 equiv) by syringe directly into the reaction solution and refluxed for 24 h, and the reaction mixture

changed from dark green to dark red. Additional PBr_3 (2.85 and 2.14 mL, 35 equiv) was added, and the reaction was refluxed another 24 h. The reaction mixture was cooled to room temperature, and methanol was added by syringe to quench the reaction, upon which the solution became dark green. The two reaction mixtures were combined and reduced under vacuum to dryness. The remaining dark brown-green solid was dissolved in CH_2Cl_2 and filtered through a Büchner funnel, and the filtrate was reduced to dryness. The residual solid was purified via chromatography with 99:1 CH_2Cl_2/MeOH on silica gel (R_f = 0.55) and dried to yield a lustrous green solid (1.34 g, 62%). All characterization data match the previously reported literature.[1]

$MeOP_8CzH_3$—To a solution of [P^V($MeOP_8Cz$)(OH)][OH] (0.105 g, 0.0862 mmol) in 30 mL of liquid ammonia at −78 °C was added sodium metal (0.0595 g, 2.59 mmol), and the mixture was stirred for 30 min. THF (20 mL) was added to the reaction mixture, and the solution was stirred for an additional 40 min at −78 °C. The reaction solution turned from dark green to a dark purple. NH_4Cl (0.641 g, 12.0 mmol) was added to the reaction mixture and was allowed to warm to room temperature to remove the ammonia. The reaction solution was filtered through a Büchner funnel, and the filtrate was removed in vacuo. A flash silica column was run with 95:5 CH_2Cl_2/EtOAc (R_f = 0.93) to separate the desired product from unreacted starting material. A flat green solid (0.0175 g, 17.6%) was obtained. The solid was used without any further purification. UV–vis (pyridine): λ_{max} (nm) 467, 671. UV–vis (CH_2Cl_2): λ_{max} (nm) 452, 623, 664, 684. LDI-MS (pyridine) m/z = 1150.8 calcd for $C_{72}H_{59}N_7O_8$ 1150.31.

TBP_8CzH_3—To a mixture of [P(TBP_8Cz)(OH)][(OH)] (0.150 g, 0.106 mmol) in 15 mL of liquid ammonia cooled to −78 °C was added sodium metal (0.090 g, 3.9 mmol) and the mixture was stirred for 30 min. THF (10 mL) was added and the mixture was stirred for an additional 30 min at −78 °C. The reaction solution turned from dark green to a red-brown. NH_4Cl (0.750 g, 14.0 mmol) was added to the reaction mixture, and the solution was allowed to slowly warm to room temperature to remove the ammonia. The reaction solution was filtered through a Büchner funnel, and the filtrate was removed in vacuo. A flash silica column was run with 40:60 hexanes/CH_2Cl_2 (R_f = 0.75) to yield a flat green solid (0.067 g, 47%). All characterization data match the previously reported literature.[1]

[(TBP_8CzH_3)(H)][BArF]—To a solution of the TBP_8CzH_3 (15 mg, 11 μmol) in 750 μL toluene was added 1.5 equiv of HBArF. A color change from green to brown was observed. This solution was layered with *n*-heptane, and X-ray quality crystals were obtained after a week. ^{1}H NMR (400 MHz, CD_2Cl_2) δ (ppm) 12.68 (vbs, 1H, Cz-*H*), 7.91 (d, $^3J_{HH}$ = 8 Hz, 4H, Ar-*H*), 7.82 (d, $^3J_{HH}$ = 8 Hz, 12H, Ar-*H*), 7.70 (d, $^3J_{HH}$ = 8 Hz, 4H, Ar-*H*), 7.61 (d, $^3J_{HH}$ = 8 Hz, 4H, Ar-*H*), 7.53 (d, $^3J_{HH}$ = 8 Hz, 4H, Ar-*H*), 7.24 (d, $^3J_{HH}$ = 8 Hz, 4H, Ar-*H*), 2.47 (s, 2H, Cz-*H*), 1.49, 1.48, 1.44, 1.30 (each a s, each 18H, *t*-Bu-*H*). UV–vis (CH_2Cl_2): λ_{max} (nm) 450, 740. LDI-MS m/z = [M]$^+$ 1360.82 calcd for $C_{96}H_{108}N_7$ 1359.88.

Mn^{III}(HOMe)($MeOP_8Cz$)—$MeOP_8CzH_3$ (0.0175 g, 0.0152 mmol) was dissolved in 10 mL of CH_2Cl_2 and 1 mL of pyridine. $Mn(acac)_3$ (0.0543 g, 0.154 mmol; acac = acetylacetonate) was added to the reaction mixture and was stirred for 12 h in the dark under air. The solvent

was removed in vacuo to yield a brown solid. The crude brown solid was purified by flash chromatography on silica gel with 8:2 CH_2Cl_2/EtOAc (R_f = 0.80). The product was dried and crystallized from $CHCl_3$:MeOH to yield Mn^{III}(HOMe)($MeOP_8Cz$) as a brown crystalline solid (0.0081 g, 43% yield). CV data (CH_2Cl_2, 100 mV) $E_{1/2}$ = 0.198 V, $E_{1/2}$ = 0.678 V, $E_{1/2}$ = −1.71 V. UV–vis (CH_2Cl_2) λ_{max} [nm] ($\varepsilon \times 10^{-4}$ M^{-1} cm^{-1}) 446 (5.50), 690 (2.48) with methanol as the axial ligand. UV–vis ($CHCl_3$) λ_{max} [nm] ($\varepsilon \times 10^{-4}$ M^{-1} cm^{-1}) 454 (5.96), 646 (1.12), 699 (1.53) with pyridine as the axial ligand. Anal. Calcd for $C_{72}H_{60}N_7O_9Mn{\cdot}0.5CHCl_3$: C, 69.01; H, 4.51; N, 7.77. Found: C, 69.29; H, 4.85; N, 7.68%. LDI-MS m/z = [M – HOMe]$^+$ 1202.49 calcd for $C_{72}H_{56}N_7O_8Mn$ 1202.22.

Mn^V(O)($MeOP_8Cz$)—Mn^{III}($MeOP_8Cz$)(HOMe) (0.0065 g, 0.0053 mmol) was dissolved in 2 mL of $CHCl_3$. PhIO (0.0028 g, 0.013 mmol) was added, and the reaction mixture was stirred for 15 min, during which time the solution slowly went from a dark brown to a dark green. The solution was filtered through glass wool and dried. The dark green-brown solid was washed with NCMe and dried. The remaining solid was purified by flash chromatography on silica column with 9:1 $CHCl_3$/EtOAc (R_f = 0.76). The product was dried under vacuum to yield a dark green solid (0.0014 g, 22% yield). ^{1}H NMR (400 MHz, CD_2Cl_2) δ 8.42 (d, $^3J_{HH}$ = 8 Hz, 4H, Ar-*H*), 8.36 (d, $^3J_{HH}$ = 8 Hz, 4H, Ar-*H*), 8.21 (d, $^3J_{HH}$ = 8 Hz, 4H, Ar-*H*), 7.42 (bs, 4H, Ar-*H*), 7.22 (d, $^3J_{HH}$ = 8 Hz, 8H, Ar-*H*), 7.12 (d, $^3J_{HH}$ = 8 Hz, 4H, Ar-*H*), 6.68 (d, $^3J_{HH}$ = 8 Hz, 4H, Ar-*H*), 4.01, 4.00, 3.95, 3.91 (each a s, each 6H, Ar-OC*H*$_3$). CV (CH_2Cl_2, 25 mV) $E_{1/2}$ = 0.07 V, $E_{1/2}$ = 0.45 V, $E_{1/2}$ = −0.57 V. UV–vis (CH_2Cl_2) λ_{max} [nm] ($\varepsilon \times 10^{-4}$ M^{-1} cm^{-1}) 436 (4.53), 636 (1.54). LDI-MS m/z = 1217.008 calcd for $C_{72}H_{56}MnN_7O_9$ 1217.352.

Kinetics Studies. General procedure

The pseudo-first-order rate constants k_{obs} were obtained by nonlinear least-squares fitting of the plots of both the growth of Mn^{III}($MeOP_8Cz$) and decay of Mn^V(O)($MeOP_8Cz$) absorbances (Abs) versus time (t) according to the equation $Abs_t = Abs_f + (Abs_0 - Abs_f)\exp(-k_{obs}t)$, where Abs_0 and Abs_f are initial and final absorbance, respectively. Second-order rate constants (k) were obtained from the slope of the best-fit line from a plot of k_{obs} versus substrate concentration. The same kinetics analysis was employed for the stopped-flow UV–vis studies. Pseudo-first-order k_{obs} values were obtained and exhibited a linear correlation with substrate concentrations.

Reaction of Mn^V(O)($MeOP_8Cz$) with C–H Substrates

Mn^V(O)($MeOP_8Cz$) (30 μM, CH_2Cl_2) was reacted with 1,4-cyclohexadiene (1,4-CHD; 0.20–1.0 mM), Xn (0.26–1.5 mM), or $AcrH_2$ (0.31–6.7 mM). The spectral changes showed isosbestic conversion of Mn^V(O)($MeOP_8Cz$) (λ_{max} = 436 and 636 nm) to Mn^{III}($MeOP_8Cz$) (λ_{max} = 446 and 689 nm).

Reaction of Mn^V(O)($MeOP_8Cz$) with Triarylphosphines

Mn^V(O)($MeOP_8Cz$) (16–30 μM, CH_2Cl_2) was reacted with varying amounts of substituted triarylphosphine (0.20–1.5 mM). The spectral changes showed isosbestic conversion of Mn^V(O)($MeOP_8Cz$) (λ_{max} = 436 and 636 nm) to Mn^{III}($MeOP_8Cz$)($OPAr_3$) (λ_{max} = 444 and 690 nm).

RESULTS AND DISCUSSION

Synthesis of Symmetrically Substituted Porphyrazines

Both symmetrically and asymmetrically substituted porphyrazines have been synthesized by using a variety of strategies.[37,48,55,58–60] The synthesis of porphyrazines typically begins with an appropriate dinitrile precursor, which is then either directly cyclized into the porphyrinoid product, or first converted to a more reactive pyrroline intermediate. In our earlier work, we relied upon a general procedure that followed the pyrroline method for the synthesis of the *p*-*tert*-butyl-substituted porphyrazine,[1] although we did not report the step-by-step details of this synthesis. Herein we describe the detailed syntheses of symmetrically substituted metal-free porphyrazines with eight *p*-substituted phenyl groups attached at the *β*-carbon atoms, RP_8PzH_2 (R = *p*-*tert*-butylphenyl (*t*-Bu), *p*-methoxyphenyl (MeO), *p*-isopropylphenyl (*i*Pr)), on a large (3–7 g) scale. These syntheses involve a new method that does not require the pyrroline step, as shown in Scheme 1. Note that the *p*-methoxyphenyl derivative was reported previously with Mg^{II} or P^{V} as the central atom, but these compounds were made by the more tedious pyrroline method on a much smaller scale, and no report of the metal-free compound was made.[37,54]

As shown in Scheme 1, the first step involves preparing the dinitrile precursor by an oxidative coupling of the phenyl-acetonitrile derivative. The reaction of 4-R-phenylacetonitrile (R = *t*-Bu, MeO, or *i*Pr) in the presence of excess NaOMe and I_2 leads to the dinitrile product.[48,53] This product crashes out of solution when cooled, and is then collected by filtration, thoroughly washed with methanol and water to remove any unreacted starting materials and impurities, and dried under vacuum to yield the dinitrile as a white or yellow solid (*t*-Bu: 75%; MeO: 61%; *i*Pr: 74%).

Two different methods to synthesize the metal-free porphyrazine from the dinitrile are shown in Scheme 1. The conventional method for synthesizing metal-free porphyrazine involves converting the dinitrile starting material into the pyrroline-2,5-diimine (blue pathway, Scheme 1), which was the original synthesis employed for TBP_8PzH_2.[1,48,54] This method involves a high-temperature reaction with ethylene glycol and a large excess of ammonia gas, giving the pyrroline product in reasonable yields (*t*-Bu: 51%; MeO: 73%). The pyrroline is then cyclized in refluxing *n*-BuOH with a Mg^{II} template. The mechanism of the cyclization has been discussed previously for phthalocyanines and triazatetrabenzcorroles.[57] The cyclized product, RP_8PzMg, is isolated by vacuum distillation and demetalated by treatment with excess TFA to form the metal-free porphyrazine as a fluffy solid, RP_8PzH_2 (*t*-Bu: 63%; MeO: 53%). Although this pathway yields the desired porphyrazines, it has significant drawbacks. The synthesis of the pyrroline requires the use of large quantities of highly reactive and toxic NH_3(g), and the yields of pyrroline are highly variable. Purification of the pyrroline is hampered by the difficulties of removing viscous and high-boiling ethylene glycol. The yields of porphyrazine also vary greatly, depending upon the quality of the Mg/butanol suspension, which is sensitive both to moisture and the quality of the magnesium source.

A new, more efficient strategy to synthesize the symmetrically substituted porphyrazines was devised that avoids the pyrroline step and can be performed on a much larger scale. Our

new synthetic strategy is based on the synthesis of certain phthalocyanine and mixed phthalocyanine-porphyrazine hybrids. [57] The method involves direct cyclization of dinitrile, avoiding the preparation of the pyrroline precursor. The dinitrile is cyclized in a mixture of 1-octanol and 1-pentanol (5:1 v/v) around a Mg^{II} template at high temperature (180 °C). Heating of dinitrile in this mixture gives Mg^{II} porphyrazine for the *i*Pr and *t*-Bu derivatives, after 2–3 h, and the MeO derivative, after 24 h (Scheme 1). The Mg^{II} porphyrazine is then isolated by vacuum distillation and purified by simple solvent extraction (MeOH) without the need for column chromatography. We optimized this procedure to work on a large scale, typically 5–7 g of dinitrile, compared to the ~1 g maximum scale of the pyrroline pathway.[1] The final metal-free porphyrazine was obtained by stirring MgPz in TFA followed by workup to yield R_8PzH_2 as a dark solid in good yield (*t*-Bu: 52%; MeO: 55%; *i*Pr: 82%.) This method takes 2–3 days, compared to the pyrroline pathway, which takes at least one to two weeks to convert the dinitrile to metal-free porphyrazine.

Synthesis of TBP_8CzH_3

The preparation of the first metal-free corrolazine, TBP_8CzH_3, was reported by us in 2001.[1] However, a complete detailed synthesis of the corrolazine, beginning from commercially available reagents, was not given in a single, convenient report. In the current work we fill in this gap by describing the complete, detailed synthesis of metal-free corrolazine from commercial precursors (Scheme 2). The synthesis has also been significantly improved since the initial report, including the improved method of porphyrazine synthesis described above. The corrolazine synthesis begins with the “ring contraction” of metal-free porphyrazine by refluxing with excess PBr_3 in pyridine for 2 d. The PBr_3 needs to be added in successive amounts (35 equiv), with a 24 h period of reflux between each addition. These conditions lead to extrusion of a *meso*-N atom and reclosure of the ring around a phosphorus template, which is inserted in the internal cavity. The mechanism of the ring contraction has been discussed, and it is proposed that the first step is insertion of the phosphorus to yield a phosphorus porphyrazine (observed in LDI-MS), followed by ring contraction via nucleophilic attack of PBr_3 at the *meso* nitrogen to form $[PNBr_3]^-$ and the desired phosphorus corrolazine.[61] After workup, the crude product is purified on a silica gel column (eluent 99:1 CH_2Cl_2/MeOH), yielding the phosphorus(V) corrolazine $[P^V(TBP_8Cz)(OH)]$-OH (confirmed by ^{31}P NMR spectroscopy) as a shiny, dark green solid (62%).

Removal of the P^V ion is challenging, since the usual methods of porphyrin demetalation involving strong acids do not work.[1] However, $[P^V(TBP_8Cz)(OH)]OH$ can be demetalated via reduction. Reaction of the P^V compound with sodium metal in NH_3/THF at −78 °C followed by quenching with NH_4Cl and warming to room temperature yields a bright green solution of crude metal-free corrolazine. Purification on silica with 60:40 CH_2Cl_2/hexanes yields TBP_8CzH_3 as a dark green solid (47%).

Protonation and Crystal Structure of TBP_8CzH_3

Numerous attempts to crystallize the metal-free corrolazine led only to precipitation of amorphous solid. However, we knew from previous work that $Mn^{III}(TBP_8Cz)$ can be monoand diprotonated at the *meso*-nitrogen positions by addition of a strong acid source, and these protonated forms were amenable to crystallization for single crystal X-ray

diffraction (XRD) studies.[32] Thus, we attempted the protonation of the metal-free compound, and found that addition of HBArF (1 equiv) (BArF = tetrakis[3,5-bis(trifluoromethyl)phenyl)borate) to a CH_2Cl_2 solution of TBP_8CzH_3 resulted in a color change from green to red, with distinct shifts in the UV–vis spectrum (Figure 2). Both Soret and Q-bands are red-shifted, with a more dramatic shift observed for the Q-band. These shifts are consistent with protonation of a *meso*-nitrogen atom on the corrolazine ring.[23,32,56,62–64] Layering of a toluene solution of $[TBP_8CzH_4][BArF]$ with *n*-heptane gave dark-colored crystals after one week. The crystal structure of the monoprotonated metal-free $[TBP_8CzH_4][BArF]$ is shown in Figure 3. Only a few crystal structures of metal-free porphyrazine[65] or corrole[2,66–71] have been reported, and the structure in Figure 3 is the first example of a crystallographically characterized metal-free corrolazine. A single BArF counterion was found in the asymmetric unit, which, by charge considerations, indicate monoprotonation of the corrolazine ring. The C–C and C–N bond distances of the corrolazine ligand in $[TBP_8CzH_4][BArF]$ are similar to those of $Mn^{III}(TBP_8Cz)$, $[Mn^{III}(TBP_8Cz(H))]$-[BArF], and $[Mn^{III}(TBP_8Cz(H)_2)][BArF]_2$,[1] indicating that the aromaticity of the ligand is not disrupted upon protonation (Figure S4 and Table S1). The four acidic protons associated with $[TBP_8CzH_4]^+$ were located unambiguously from difference Fourier maps. Surprisingly, only two of the pyrrole N–H protons were located inside the corrolazine cavity. The third pyrrole N–H proton was located on a *meso*-N atom, along with the additional proton from HBArF, which was found on the opposite *meso*-nitrogen. An edge-on view of the structure is shown in Figure 3, revealing a planar macrocycle, with the two NH protons on opposite sides of the cavity. In contrast, the structures of metal-free corroles are significantly puckered due to the steric strain of the three pyrrolic N–H protons in the internal cavity.[2,66–71]

Synthesis of $MeOP_8CzH_3$

The new corrolazine $[P^V(MeOP_8Cz)(OH)]OH$ was prepared by a route similar to $[P^V(TBP_8Cz)(OH)]OH$, with a slight modification of the PBr_3 ring-contraction step (see Experimental). Purification on silica with CH_2Cl_2/EtOAc (8:2 v/v) yields the ring-contracted product as a flat green solid (49%; Scheme 2). The UV–vis spectrum for $[P^V(MeOP_8Cz)(OH)]OH$ yields two diagnostic peaks expected for a corrolazine ring, a Soret band at 461 nm ($\varepsilon = 8.2 \times 10^4\ M^{-1}\ cm^{-1}$), and a Q-band at 644 nm ($\varepsilon = 4.5 \times 10^4\ M^{-1}\ cm^{-1}$; (Figure 4). The ^1H NMR spectrum (Figure S9) supports the formation of a symmetric product, with four singlets found upfield (~4 ppm) that can be assigned to the *p*-MeO groups and eight resonances in the aromatic region, each integrating to 2H as expected for the different phenyl protons. A single resonance is observed at −111.35 ppm in the ^{31}P NMR spectrum, which is in agreement with other five coordinate phosphorus corrole and corrolazine complexes.[1,41,42] Both LDI-MS and elemental analysis were also consistent with the structure of the final product.

Further characterization of $[P^V(MeOP_8Cz)(OH)]OH$ via cyclic voltammetry revealed two reversible waves, and one quasi-reversible wave, at −1.78, −1.27, and 0.65 V versus Fc^+/Fc, respectively (Figure 5). These data can be compared to the electrochemical data for $[P^V(TBP_8Cz)(OH)]OH$, which exhibits three waves at −1.70, −1.25, and 0.71 V versus Fc^+/Fc.[1] The *p*-MeO substituents cause a negative shift in all three redox potentials, with the

largest shift being 80 mV for the second reduction wave. The data show that substitution of *p*-*t*-Bu for *p*-MeO groups influences both ring-based and metalbased redox potentials, indicating that the MeO derivative is more electron-rich than the *t*-Bu compound.

Crystals of $P^{V}(MeOP_8Cz)(OMe)_2$ suitable for XRD were obtained via slow diffusion of MeOH into a CH_2Cl_2 solution of $[P^{V}(MeOP_8Cz)(OH)]OH$. The structure of $P^{V}(MeOP_8Cz)$-$(OMe)_2$ reveals the expected ring-contracted product, with an octahedral phosphorus that has two methoxy groups bound in axial positions (P–O9 = 1.6996(19) Å; P–O10 = 1.6792 (19) Å; Figure 6, Table 1). The phosphorus atom is nearly coplanar with the corrolazine ligand, sitting 0.012 Å above the plane defined by the pyrrole-N atoms, and 0.051 Å above the plane defined by the 23-atom macrocyclic core. This is more in the plane of the corrolazine by 0.022 and 0.014 Å compared to the $P^{V}(TBP_8Cz)(OMe)_2$. The N6–P–N7 bond angle of 83.23(9)°, which includes the pyrroles involved in the C*α*–C*α* linkage, is ca. 12° smaller than the opposite angle N2–P–N4, as seen for the *t*-Bu derivative. The average P–N bond distance (1.78 Å) is also comparable to $P^{V}(TBP_8Cz)(OMe)_2$ (1.77 Å).

The ^{31}P NMR of $P^{V}(MeOP_8Cz)(OMe)_2$ shows an upfield signal at −192.7 ppm compared to −111.4 ppm for the five-coordinate complex before crystallization. This upfield shift is well-documented for six-coordinate phosphorus(V) porphyrazines and corrolazines.[1,37,41,72] Addition of water converts the six-coordinate complex back to the five-coordinate $[P^{V}(MeOP_8Cz)(OH)]OH$ (along with some side products) as confirmed by ^{31}P NMR.

Manganese Derivatives of *p*-Methoxyphenyl-Substituted Corrolazine

The complex $[P^{V}(MeOP_8Cz)(OH)]OH$ was demetalated with liquid NH_3 in the presence of excess sodium metal at −78 °C. The desired metal-free product could be partly purified by column chromatography on silica gel (eluent 95:5 CH_2Cl_2/EtOAc), yielding material of sufficient purity to be carried on to the next step. Metal-free $MeOP_8CzH_3$ was reacted with $Mn(acac)_3$ in CH_2Cl_2/pyridine (10:1 v/v) by stirring for 12 h in the dark (Scheme 2). The metalated product, $Mn^{III}(MeOP_8Cz)$, was purified via flash chromatography and recrystallized from layering of a $CHCl_3$ solution of $Mn^{III}(MeOP_8Cz)$ with MeOH to yield $Mn^{III}(MeOP_8Cz)$-(HOMe) as a dark brown crystalline solid (43%). The UV–vis spectrum of $Mn^{III}(MeOP_8Cz)(HOMe)$ reveals a Soret band at 446 nm ($\varepsilon = 5.50 \times 10^4\ M^{-1}\ cm^{-1}$) and a Q-band at 690 nm ($\varepsilon = 2.48 \times 10^4\ M^{-1}\ cm^{-1}$) as seen in Figure 7, together with the *t*-Bu derivative for comparison (vide infra). Addition of pyridine causes a significant shift in the Soret and Q-bands to 454 ($\varepsilon = 5.96 \times 10^4\ M^{-1}\ cm^{-1}$) and 699 nm ($\varepsilon = 1.53 \times 10^4\ M^{-1}\ cm^{-1}$), respectively, consistent with axial coordination of pyridine to $Mn^{III}(MeOP_8Cz)$. The pyridine spectrum also matched those seen for aliquots taken from the reaction mixture during metalation.

The cyclic voltammogram for $Mn^{III}(MeOP_8Cz)(HOMe)$ in CH_2Cl_2 yields three quasi-reversible waves at 0.68, 0.20, and −1.71 V versus Fc^{+}/Fc (Figure 8). The wave at 0.20 V can be assigned to a metal-based oxidation, whereas the other two processes are likely ring-based. The wave at −1.71 V can be assigned to one-electron reduction of the corrolazine ring. For comparison, the cyclic voltammogram for $Mn^{III}(TBP_8Cz)$ was obtained in the same solvent, CH_2Cl_2 (Figure S12). Three quasi-reversible waves were observed for the *t*-Bu derivative at potentials of 0.76, 0.28, and −1.67 V. The shift in potentials for the MeO

derivative is indicative of this system being more electron-rich compared to the *t*-Bu derivative, as expected for substitution of *t*-Bu by MeO on the eight aryl peripheral substituents.

Crystals of $Mn^{III}(MeOP_8Cz)(MeOH)$ led to the structure shown in Figure 9. Selected bond lengths and angles are given in Table 2 together with those of $Mn^{III}(TBP_8Cz)(MeOH)$ for comparison. The complex crystallizes with one axial methanol ligand (Mn–O = 2.130(5) Å). The bond distances and angles around the metal ion for $Mn^{III}(MeOP_8Cz)(MeOH)$ are similar to the phosphorus derivative $P^{V}(MeOP_8Cz)(MeO)_2$ and $Mn^{III}(TBP_8Cz)(MeOH)$,[47] but the Cα-Cα linkage is smaller than that seen for $P^{V}(MeOP_8Cz)(MeO)_2$ (1.423(3) Å) or the *t*-Bu derivative (1.445(6) Å). The origin of this Cα–Cα linkage shortening for the MeO derivative is not known.

The complex $Mn^{III}(MeOP_8Cz)(MeOH)$ was converted into a high-valent $Mn^{V}(O)$ complex by oxidation with iodosylbenzene. $Mn^{III}(MeOP_8Cz)(MeOH)$ was mixed with 2.5 equiv of PhIO, as shown in Scheme 3. The heterogeneous reaction mixture went from a dark brown to a bright green in color, indicating formation of $Mn^{V}(O)(MeOP_8Cz)$, which was purified by column chromatography and isolated as a stable dark green solid (22%). The UV–vis spectrum for $Mn^{V}(O)$-$(MeOP_8Cz)$ is similar to that seen for $Mn^{V}(O)(TBP_8Cz)$, with a Soret band at 440 nm ($\varepsilon = 4.52 \times 10^4\ M^{-1}\ cm^{-1}$) and a blueshifted, broad, and relatively weak Q-band at 636 nm ($\varepsilon = 1.54 \times 10^4\ M^{-1}\ cm^{-1}$; Figure 10).[47] The complex $Mn^{V}(O)$-$(MeOP_8Cz)$ was characterized by ^1H NMR spectroscopy and LDI-MS. A diamagnetic ^1H NMR spectrum (Figure S13) was observed, with four singlets appearing at 4.00–3.95 ppm for the *p*-MeO substituents, and a total of seven resonances between 8.4 and 6.7 ppm assigned to the eight peripheral aryl substituents. The NMR spectrum confirms the diamagnetic, low-spin, d^2 configuration of the metal. The stability of the *p*-MeO-substituted $Mn^{V}(O)$ complex is the same as the *t*-Bu derivative, allowing for long-term storage of $Mn^{V}(O)$-$(MeOP_8Cz)$. The influence of the *p*-MeO substituents on the redox properties of the $Mn^{V}(O)$ complex was assessed. The cyclic voltammogram of $Mn^{V}(O)(MeOP_8Cz)$ is shown in Figure 11. There are two major redox processes that can be seen at $E_{1/2} = 0.45$ and −0.57 V, which can be assigned to ring oxidation and metal reduction, respectively, based on previous redox assignments for metallocorrolazines.[47] There is also a small redox couple centered at $E_{1/2} =$ 0.07 V, which likely arises from a small amount of an unidentified impurity. The Mn^{V}/Mn^{IV} redox couple is shifted in the negative direction by 40 mV when compared to $Mn^{V}(O)$ (TBP_8Cz), and the corrolazine ring oxidation has shifted by 60 mV in the same direction.[24] The shifts indicate that the remote *p*-MeO substituents increase the electron density at the metal center.

Comparison of Spectroscopic and Redox Properties with Other Porphyrinoid Compounds

A comparison of the UV–vis data for the complexes in this study together with other porphyrinoid compounds is useful to understand the electronic influence of the peripheral aryl groups on the corrolazine ring. In all cases, a red shift was observed for both the Soret and Q-bands for the MeO-substituted corrolazines as compared to the *t*-Bu-substituted compounds, and the extinction coefficients for the MeO compounds are found to be smaller for both bands (Table 3). This observation can be compared to what was reported by

Kobayashi for a series of related magnesium and phosphorus octa-aryl-porphyrazines, in which it was shown that an increase in the electron-donating ability of the peripheral aryl groups caused a red shift in the Q-bands. [37] These observations are in contrast to what is seen for both *meso*-aryl-[34,73] and *β*-aryl-substituted porphyrins,[35,74] which show no clear correlation with the electron-donating properties of the substituents and the UV–vis transitions. However, the magnitude of the shifts observed for the Q-bands in porphyrazines are slightly larger than those seen for the corrolazines, whereas the opposite trend is seen for the Soret bands, in which the corrolazines show a more pronounced effect.

With regard to redox potentials, the MeO corrolazine complexes uniformly show shifts to more negative potentials when compared to the analogous *t*-Bu corrolazines. The redox potentials of metalloporphyrins are also sensitive to substitution of the *para*-position on aryl groups attached at the *meso* positions, but the magnitude of the shifts are highly dependent on the identity of the metal center.[35,73,75–77] In contrast, the changes in redox potentials from *para* substitution in the corrolazine complexes are relatively insensitive to the identity of the internal metal, although the substituents for the corrolazine compounds are attached at the *β*-carbon atoms and not the *meso* positions. To our knowledge, there is only one study describing the *para*-R substitution (R = H, F) of aryl rings attached at the *β*-carbon atoms of a porphyrin. In this case, the manganese(III) octaaryl porphyrins exhibited a shift in both metal- and porphyrin-based redox potentials (50–80 mV) that is similar in magnitude to that seen for the corrolazines.[78]

Reactivity of $Mn^{V}(O)$ Corrolazines. Hydrogen-Atom Transfer with C–H Substrates

The reactivity of $Mn^{V}(O)$-($MeOP_8Cz$) with a variety of substrates containing C–H bonds was examined to determine how changing the redox potential at the metal center effects the rate of hydrogen atom transfer (HAT) (Scheme 4). The reaction of $Mn^{V}(O)(MeOP_8Cz)$ with excess C–H substrates in CH_2Cl_2 was monitored by UV–vis spectroscopy (Figure 12). The Q-band for the $Mn^{V}(O)$ complex at 636 nm decays over time along with the isosbestic growth of a peak at 689 nm corresponding to the formation of $Mn^{III}(MeOP_8Cz)(H_2O)$. Plots of absorbance versus time for both species, $Mn^{V}(O)(MeOP_8Cz)$ and $Mn^{III}(MeOP_8Cz)$, yield single exponential curves that are well-fit by pseudo-first-order kinetics, yielding the pseudo-first-order rate constants (k_{obs}). The rate constants increased with increasing concentration of substrate, and plots of k_{obs} versus [C–H substrate] provided a linear relationship whose slope gives the second-order rate constants (Table 4).

As seen in Table 4, the largest difference in HAT rates for the MeO and *t*-Bu derivatives is observed with 1,4-CHD, in which there is a twofold rate enhancement for the MeO-substituted complex. For the other substrates (Xn, $AcrH_2$), there is little or no change in reaction rates for the two corrolazine derivatives. For $Mn^{V}(O)$ complexes, the HAT rates decrease with increasing C–H bond strength,[79] as expected for an HAT mechanism.[26] The driving force for HAT can be related to the bond strength of the O–H bond being formed in the MnO–H product. This bond strength can in turn be related to the redox potential and basicity of the one-electron-reduced $[Mn^{IV}(O)]^{-}$ species through eq 1:

$$\mathrm{BDFE}(\mathrm{Mn^{IV}O{-}H}) = 1.37\mathrm{p}K_a + 23.06E^\circ + C_G \quad (1)$$

where BDFE = bond dissociation free energy of the O–H bond formed, the pK_a and $E°$ equal the basicity of $[Mn^{IV}(O)]^-$ and the $Mn^{V/IV}(O)$ couple, respectively, and C_G is the free energy of formation of a hydrogen atom.[80–82] The lower redox potential of the MeO derivative should contribute to a weaker Mn^{IV}O–H bond by ~1 kcal/mol and hence lead to a slightly *weaker* driving force for HAT. However, the data in Table 4 show that the rates of HAT for MeO versus *t*-Bu complexes are slightly *greater* for the MeO derivative. These data suggest that the basicity of the $[Mn^{IV}(O)]^-$ species is enhanced for the MeO derivative, thereby compensating for the lower redox potential and increasing the driving force for HAT.

Oxygen-Atom Transfer with Triarylphosphines

The reaction of $Mn^V(O)(MeOP_8Cz)$ with excess triarylphosphine derivatives in CH_2Cl_2 was monitored by UV–vis spectroscopy (Figure 12). The disappearance of $Mn^V(O)(MeOP_8Cz)$ (436, 636 nm) was seen together with the isosbestic growth of $Mn^{III}(MeOP_8Cz)(OPAr_3)$ (444, 690 nm), consistent with the two-electron oxidation of the triarylphosphine to phosphine oxide. The formation of phosphine oxide was confirmed by ^{31}P NMR spectroscopy. The coordination of the phosphine oxide to the Mn ion is supported by the appearance of a split Soret band.[83] Plots of absorbance versus time and subsequent fitting of the data yielded the pseudo-first-order rate constants (k_{obs}), and plotting of the k_{obs} versus [PAr_3] gives a linear relationship, which provides a measure of the second-order rate constants (Table 5).

The rate constants of OAT for $Mn^V(O)(MeOP_8Cz)$ with the substituted triarylphosphines are slower than the corresponding rate constants for $Mn^V(O)(TBP_8Cz)$. The greatest difference in second-order rate constant is seen for the most electron-poor phosphine (P(*p*-CF_3–Ph)$_3$). A linear relationship ($\rho = -1.01(2)$) was observed in the Hammett plot for the reaction of the *p*-X-substituted triarylphosphines with $Mn^V(O)$-($MeOP_8Cz$) (Figure 13). A more negative ρ-value is seen for the MeO complex as compared to the *t*-Bu complex ($\rho = -0.91(5)$), and this observation is consistent with a less electrophilic *p*-MeO complex. The weakened electrophilicity correlates nicely with the lower redox potential of the latter complex. The steric influence of the substrate was studied by the use of the tri(*o*-tolyl)-substituted phosphine. A large decrease of ~3000-fold in the second-order rate constant was observed going from the tri(*p*-tolyl)phosphine to tri(*o*-tolyl)-substituted phosphine, which is similar to the ~3700-fold decrease seen for $Mn^V(O)(TBP_8Cz)$. This rate change provides strong evidence that $Mn^V(O)(MeOP_8Cz)$ reacts via a concerted oxygen-atom transfer mechanism, as does $Mn^V(O)$-(TBP_8Cz).[83] Overall, the kinetics show that the *para*-methoxy derivative in general is a weaker oxygen atom transfer agent than the *tert*-butyl derivative.

SUMMARY AND CONCLUSIONS

This work provides a general one-pot synthesis, from dinitrile to metal-free porphyrazine, for symmetrical octa-arylporphyrazines, RP_8PzH_2 (R = *t*-Bu, MeO, and *i*Pr). Furthermore,

the optimized and complete synthesis of metal-free corrolazine from commercially available reagents is presented. The detailed synthetic protocol given here should allow for easy reproducibility of corrolazine synthesis on a practical scale by other laboratories. New manganese(III) and manganese(V)-oxo corrolazines with *p*-MeO-phenyl substituents are also reported. Characterization of the *p*-MeO corrolazines by UV–vis spectroscopy and CV revealed clear effects induced by the modification of the peripheral substituents on the *β*-carbon atoms. Substitution of MeO in place of *t*-Bu leads to a red shift in the Soret and Q-bands in the UV–vis spectrum, which is consistent with a more electron-rich corrolazine. An increase in electron density at the metal center is also indicated by the CV data, where a negative shift (20–80 mV) for the $Mn^{V/IV}$ couple and the corrolazine ring oxidation is observed.

The relative hydrogen atom transfer and oxygen atom transfer chemistry of Mn^{V}(O)($MeOP_8Cz$) versus Mn^{V}(O)-(TBP_8Cz) was determined. The Mn^{V}(O)($MeOP_8Cz$) complex was found to abstract hydrogen atoms from activated C–H bonds. The rate of HAT was either the same or slightly faster for Mn^{V}(O)($MeOP_8Cz$) than for Mn^{V}(O)(TBP_8Cz). The rate acceleration for HAT observed for the *p*-MeO derivative contradicts the prediction that slower rates of HAT should follow from the lower $Mn^{V/IV}$ redox potential for this complex. A reasonable explanation for the HAT reactivity is that the *p*-MeO substituents enhance the basicity of the putative $[Mn^{IV}(O)]^{-}$, thereby increasing the driving force for HAT, which compensates for the lower redox potential. This result can be compared to previous studies from our group that showed that the addition of anionic axial donors to Mn^{V}(O)-(TBP_8Cz) also showed enhanced rates of HAT, and this increase was attributed to the same increase in basicity and overall driving force.[26] These studies provide support for the notions that the basicity of high-valent metal-oxo porphyrinoid species plays a major role in determining reactivity and that biological systems can use different strategies to tune this parameter involving both porphyrinoid structure and axial ligand effects.

The OAT reactivity for Mn^{V}(O)($MeOP_8Cz$) is lower than that seen for Mn^{V}(O)(TBP_8Cz) with the same substrates. The *p*-MeO derivative exhibits slower OAT rate constants with triarylphosphine substrates, and the observed lower reactivity is consistent with Mn^{V}(O)($MeOP_8Cz$) being less electrophilic. This result contrasts the dramatic increase in OAT rates seen for the addition of anionic axial ligands to Mn^{V}(O)-(TBP_8Cz).[27,28] One might predict that the addition of an electron-donating axial donor would cause an effect similar to that seen for the addition of an electron-donating group to the equatorial peripheral substituents. However, instead of the decrease in OAT rates seen for the *p*-MeO derivative, large rate enhancements for OAT (up to 24 000-fold) were observed.[27,28] This increase in OAT reactivity was attributed to stabilization of the two-electron-reduced Mn^{III} product from binding the axial ligand. In the current work we have succeeded in isolating the influence of a purely electronic effect on the rates of OAT, and in this case an increase in the electron-donating properties of the ligand slows OAT.

This work shows that the HAT and OAT reactivity of metallocorrolazines can be tuned by substitution at remote peripheral positions on the Cz ring. With the streamlined synthetic methodology described here, future work can focus on modifications to the Cz periphery to further enhance reactivity at the metal center.

Supplementary Material

Refer to Web version on PubMed Central for supplementary material.

Acknowledgments

This work was supported by the NIH (GM101153 to D.P.G). E.E.J. is grateful for The Johns Hopkins Dean's Science Postdoctoral Teaching Fellowship. J.P.T.Z. acknowledges the Glen E. Meyer '39 Fellowship for Research Support. R.A.B. is grateful for the Harry and Cleio Greer Fellowship.

References

1. Ramdhanie B, Stern CL, Goldberg DP. J Am Chem Soc. 2001; 123:9447–9448. [PubMed: 11562230]
2. Kumar A, Goldberg I, Botoshansky M, Buchman Y, Gross Z. J Am Chem Soc. 2010; 132:15233–15245. [PubMed: 20932015]
3. Abu-Omar MM. Dalton Trans. 2011; 40:3435–3444. [PubMed: 21279237]
4. Zdilla MJ, Abu-Omar MM. Inorg Chem. 2008; 47:10718–10722. [PubMed: 18855381]
5. Bougher CJ, Liu S, Hicks SD, Abu-Omar MM. J Am Chem Soc. 2015; 137:14481–14487. [PubMed: 26517943]
6. Bröring M, Hell C, Brandt CD. Chem Commun. 2007:1861–1862.
7. Bröring M, Brégier F, Krüger R, Kleeberg C. Eur J Inorg Chem. 2008; 2008:5505–5512.
8. Sakow D, Baabe D, Böker B, Burghaus O, Funk M, Kleeberg C, Menzel D, Pietzonka C, Bröring M. Chem - Eur J. 2014; 20:2913–2924. [PubMed: 24478121]
9. Czernuszewicz RS, Mody V, Czader A, Gałęzowski M, Gryko DT. J Am Chem Soc. 2009; 131:14214–14215. [PubMed: 19757774]
10. Kim SH, Park H, Seo MS, Kubo M, Ogura T, Klajn J, Gryko DT, Valentine JS, Nam W. J Am Chem Soc. 2010; 132:14030–14032. [PubMed: 20845972]
11. Rittle J, Green MT. Science. 2010; 330:933–937. [PubMed: 21071661]
12. Poulos TL. Chem Rev. 2014; 114:3919–3962. [PubMed: 24400737]
13. Jung C. Biochim Biophys Acta, Proteins Proteomics. 2011; 1814:46–57.
14. Groves JT. Nat Chem. 2014; 6:89–91. [PubMed: 24451580]
15. Boaz NC, Bell SR, Groves JT. J Am Chem Soc. 2015; 137:2875–2885. [PubMed: 25651467]
16. Takahashi A, Kurahashi T, Fujii H. Inorg Chem. 2009; 48:2614–2625. [PubMed: 19216512]
17. Takahashi A, Kurahashi T, Fujii H. Inorg Chem. 2011; 50:6922–6928. [PubMed: 21714484]
18. Fox JP, Ramdhanie B, Zareba AA, Czernuszewicz RS, Goldberg DP. Inorg Chem. 2004; 43:6600–6608. [PubMed: 15476357]
19. Ramdhanie B, Telser J, Caneschi A, Zakharov LN, Rheingold AL, Goldberg DP. J Am Chem Soc. 2004; 126:2515–2525. [PubMed: 14982461]
20. Cho K, Leeladee P, McGown AJ, DeBeer S, Goldberg DP. J Am Chem Soc. 2012; 134:7392–7399. [PubMed: 22489757]
21. Leeladee P, Jameson GNL, Siegler MA, Kumar D, de Visser SP, Goldberg DP. Inorg Chem. 2013; 52:4668–4682. [PubMed: 23527920]
22. Kurahashi S, Ikeue T, Sugimori T, Takahashi M, Mikuriya M, Handa M, Ikezaki A, Nakamura M. J Porphyrins Phthalocyanines. 2012; 16:518–529.
23. Zaragoza JPT, Siegler MA, Goldberg DP. Chem Commun. 2016; 52:167–170.
24. Baglia RA, Prokop-Prigge KA, Neu HM, Siegler MA, Goldberg DP. J Am Chem Soc. 2015; 137:10874–10877. [PubMed: 26295412]
25. Mandimutsira BS, Ramdhanie B, Todd RC, Wang H, Zareba AA, Czernuszewicz RS, Goldberg DP. J Am Chem Soc. 2002; 124:15170–15171. [PubMed: 12487581]
26. Prokop KA, de Visser SP, Goldberg DP. Angew Chem, Int Ed. 2010; 49:5091–5095.

27. Neu HM, Yang T, Baglia RA, Yosca TH, Green MT, Quesne MG, de Visser SP, Goldberg DP. J Am Chem Soc. 2014; 136:13845–13852. [PubMed: 25238495]
28. Neu HM, Quesne MG, Yang T, Prokop-Prigge KA, Lancaster KM, Donohoe J, DeBeer S, de Visser SP, Goldberg DP. Chem - Eur J. 2014; 20:14584–14588. [PubMed: 25256417]
29. Prokop KA, Neu HM, de Visser SP, Goldberg DP. J Am Chem Soc. 2011; 133:15874–15877. [PubMed: 21888343]
30. Baglia RA, Dürr M, Ivanović-Burmazović I, Goldberg DP. Inorg Chem. 2014; 53:5893–5895. [PubMed: 24873989]
31. Leeladee P, Baglia RA, Prokop KA, Latifi R, de Visser SP, Goldberg DP. J Am Chem Soc. 2012; 134:10397–10400. [PubMed: 22667991]
32. Neu HM, Jung J, Baglia RA, Siegler MA, Ohkubo K, Fukuzumi S, Goldberg DP. J Am Chem Soc. 2015; 137:4614–4617. [PubMed: 25839905]
33. Zakavi S, Omidyan R, Ebrahimi L, Heidarizadi F. Inorg Chem Commun. 2011; 14:1827–1832.
34. Ormond AB, Freeman HS. Dyes Pigm. 2013; 96:440–448.
35. Bhyrappa P, Sankar M, Varghese B. Inorg Chem. 2006; 45:4136–4149. [PubMed: 16676974]
36. Beletskaya, IP.; Tyurin, VS.; Uglov, A.; Stern, C.; Guilard, R. Handbook of Porphyrin Science;. Vol. 25. World Scientific Publishing Company; 2012. p. 81-279.
37. Furuyama T, Yoshida T, Hashizume D, Kobayashi N. Chem Sci. 2014; 5:2466–2474.
38. Yoshida T, Furuyama T, Kobayashi N. Tetrahedron Lett. 2015; 56:1671–1674.
39. Furuyama T, Harako R, Kobayashi N. J Porphyrins Phthalocyanines. 2015; 19:500–509.
40. Ivanova SS, Moryganova Y, Hamdoush M, Koifman OI, Sal'nikov DS, Stuzhin PA. J Porphyrins Phthalocyanines. 2014; 18:875–883.
41. Fox JP, Goldberg DP. Inorg Chem. 2003; 42:8181–8191. [PubMed: 14658868]
42. Zhang XF. Coord Chem Rev. 2015; 285:52–64.
43. Furuyama T, Sugiya Y, Kobayashi N. Chem Commun. 2014; 50:4312.
44. Lee CW, Lu HP, Lan CM, Huang YL, Liang YR, Yen WN, Liu YC, Lin YS, Diau EWG, Yeh CY. Chem - Eur J. 2009; 15:1403–1412. [PubMed: 19097125]
45. O'Regan BC, López-Duarte I, Martínez-Díaz MV, Forneli A, Albero J, Morandeira A, Palomares E, Torres T, Durrant JR. J Am Chem Soc. 2008; 130:2906–2907. [PubMed: 18281988]
46. Cid JJ, Yum JH, Jang SR, Nazeeruddin MK, Martínez-Ferrero E, Palomares E, Ko J, Grätzel M, Torres T. Angew Chem Int Ed. 2007; 46:8539–8362.
47. Lansky DE, Mandimutsira B, Ramdhanie B, Clausén M, Penner-Hahn J, Zvyagin SA, Telser J, Krzystek J, Zhan R, Ou Z, Kadish KM, Zakharov L, Rheingold AL, Goldberg DP. Inorg Chem. 2005; 44:4485–4498. [PubMed: 15962955]
48. Baumann TF, Barrett AGM, Hoffman BM. Inorg Chem. 1997; 36:5661–5665.
49. Fukuzumi S, Kotani H, Prokop KA, Goldberg DP. J Am Chem Soc. 2011; 133:1859–1869. [PubMed: 21218824]
50. Hijazi AK, Taha ZA, Ajlouni A, Radhakrishnan N, Voit B, Kühn FE. J Organomet Chem. 2014; 763–764:65–68.
51. Sheldrick GM. Acta Crystallogr, Sect A: Found Crystallogr. 2008; 64:112–122.
52. Spek AL. J Appl Crystallogr. 2003; 36:7–13.
53. Yeh HC, Wu WC, Wen YS, Dai DC, Wang JK, Chen CT. J Org Chem. 2004; 69:6455–6462. [PubMed: 15357608]
54. Furuyama T, Ogura Y, Yoza K, Kobayashi N. Angew Chem, Int Ed. 2012; 51:11110–11114.
55. Nie H, Barrett AGM, Hoffman BM. J Org Chem. 1999; 64:6791–6796. [PubMed: 11674688]
56. Goslinski T, Tykarska E, Kryjewski M, Osmalek T, Sobiak S, Gdaniec M, Dutkiewicz Z, Mielcarek J. Anal Sci. 2011; 27:511–515. [PubMed: 21558658]
57. Vagin SI, Hanack M. Eur J Org Chem. 2002; 2002:2859–2865.
58. Lijewski S, Piskorz J, Kucinska M, Wierzchowski M, Czerniak K, Billert H, Murias M, Mielcarek J, Goslinski T. Inorg Chem Commun. 2013; 29:97–100.
59. Ebenso EE, Mongale MK, Isabirye DA, Kabanda MM. Asian J Chem. 2013; 25:2308–2314.

60. Ovchenkova EN, Hanack M, Lomova TN. Macroheterocycles. 2010; 3:63–67.
61. Li J, Subramanian LR, Hanack M. Eur J Org Chem. 1998; 1998:2759–2767.
62. Klyueva ME, Stuzhin PA, Berezin BD. Russ J Coord Chem. 2003; 29:189–195.
63. Freyer W, Minh LQ. J Porphyrins Phthalocyanines. 1997; 1:287–295.
64. Graczyk A, Białkowskia E. Tetrahedron. 1978; 34:3505–3509.
65. Zhong C, Zhao M, Stern C, Barrett AGM, Hoffman BM. Inorg Chem. 2005; 44:8272–8276. [PubMed: 16270965]
66. Simkhovich L. J Inorg Biochem. 2000; 80:235–238. [PubMed: 11001094]
67. Harrison HR, Hodder OJR, Hodgkin DC. J Chem Soc B. 1971:640–645.
68. Paolesse R, Marini A, Nardis S, Froiio A, Mandoj F, Nurco DJ, Prodi L, Montalti M, Smith KM. J Porphyrins Phthalocyanines. 2003; 07:25–36.
69. Ding T, Harvey JD, Ziegler CJ. J Porphyrins Phthalocyanines. 2005; 09:22–27.
70. Goldschmidt R, Goldberg I, Balazs Y, Gross Z. J Porphyrins Phthalocyanines. 2006; 10:76–86.
71. Gross Z, Simkhovich L, Galili N. Chem Commun. 1999:599–600.
72. Holmes RR. Chem Rev. 1996; 96:927–950. [PubMed: 11848776]
73. Chen P, Finikova OS, Ou Z, Vinogradov SA, Kadish KM. Inorg Chem. 2012; 51:6200–6210. [PubMed: 22621652]
74. Friedman M. J Org Chem. 1965; 30:859–863.
75. Ye L, Ou Z, Fang Y, Xue S, Song Y, Wang L, Wang M, Kadish KM. RSC Adv. 2015; 5:77088–77096.
76. Kadish KM, Lin M, Caemelbecke EV, De Stefano G, Medforth CJ, Nurco DJ, Nelson NY, Krattinger B, Muzzi CM, Jaquinod L, Xu Y, Shyr DC, Smith KM, Shelnutt JA. Inorg Chem. 2002; 41:6673–6687. [PubMed: 12470062]
77. Walker FA, Beroiz D, Kadish KM. J Am Chem Soc. 1976; 98:3484–3489. [PubMed: 944733]
78. Van Caemelbecke E, Kutner W, Kadish KM. Inorg Chem. 1993; 32:438–444.
79. Warren JJ, Tronic TA, Mayer JM. Chem Rev. 2010; 110:6961–7001. [PubMed: 20925411]
80. Borovik AS. Chem Soc Rev. 2011; 40:1870–1874. [PubMed: 21365079]
81. Usharani D, Lacy DC, Borovik AS, Shaik S. J Am Chem Soc. 2013; 135:17090–17104. [PubMed: 24124906]
82. Bordwell FG, Cheng JP, Harrelson JA. J Am Chem Soc. 1988; 110:1229–1231.
83. Zaragoza JPT, Baglia RA, Siegler MA, Goldberg DP. J Am Chem Soc. 2015; 137:6531–6540. [PubMed: 25964988]

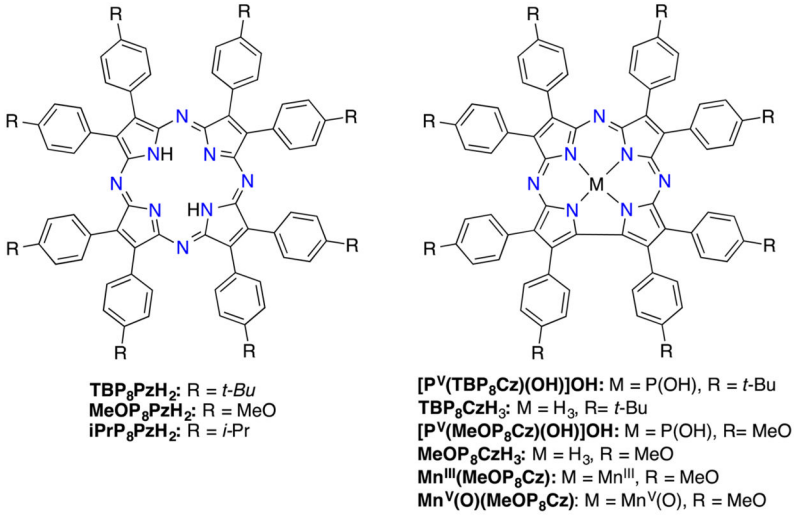

Figure 1.
General motif for porphyrazine and corrolazine complexes.

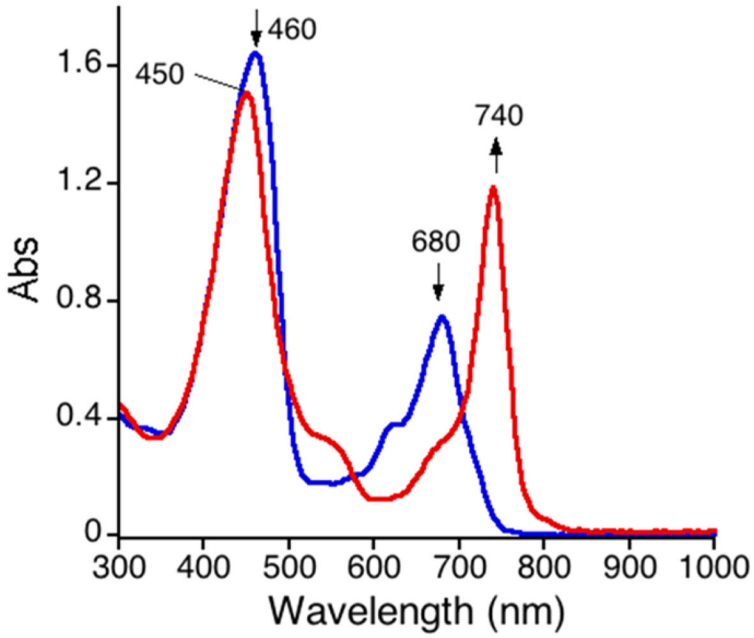

Figure 2.
UV–vis spectrum of TBP_8CzH_3 (blue line) and $[TBP_8CzH_4][BArF]$ (red line) in CH_2Cl_2.

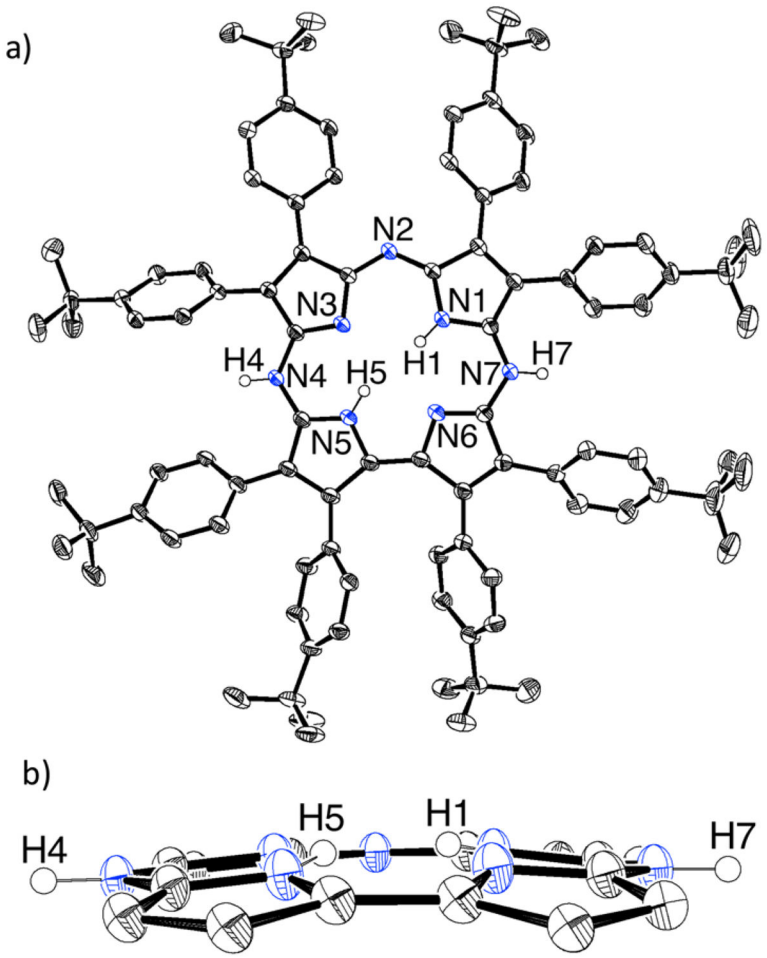

Figure 3.

(a) Displacement ellipsoid plot (50% probability level) of the $[TBP_8CzH_4]^+$ cation at 110(2) K. Hydrogen atoms, except for N–H hydrogen, and disorder are omitted for clarity. (b) Edge-on view down the plane of the Cz ring, with hydrogen atoms, except for N–H hydrogen, and *tert*-butylphenyl groups omitted for clarity.

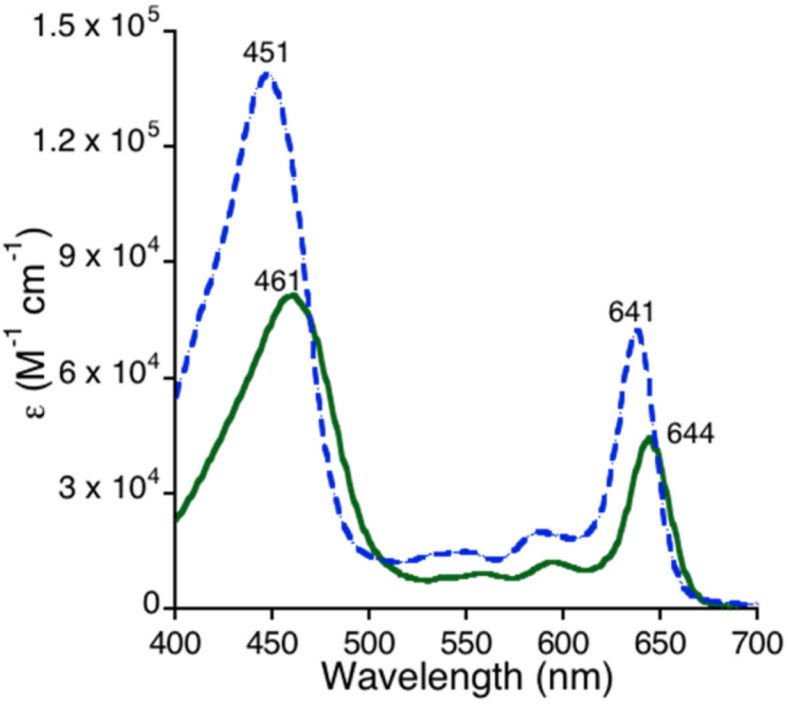

Figure 4.

UV–vis spectrum of [P^V(TBP$_8$Cz)(OH)]OH (blue dashed line) and [P^V(MeOP$_8$Cz)(OH)]OH (green solid line) in CH_2Cl_2.

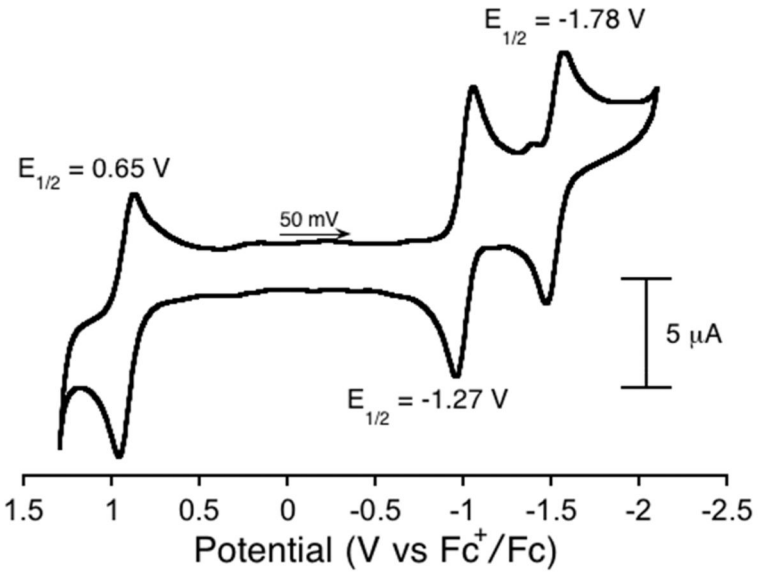

Figure 5.

Cyclic voltammogram for $[P^{V}(MeOP_8Cz)(OH)]OH$ (0.7 mM) in CH_2Cl_2 with 0.1 M $TBAPF_6$ electrolyte.

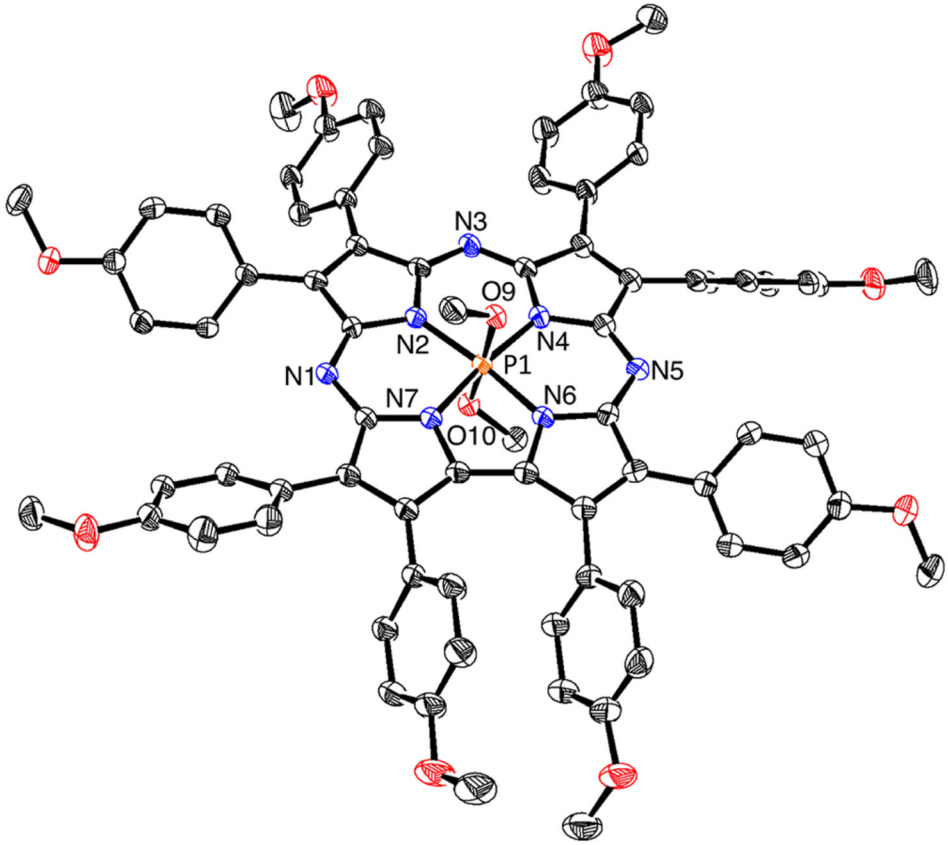

Figure 6.

Displacement ellipsoid plot (50% probability level) of $P^{V}(MeOP_8Cz)(OMe)_2$ at 110(2) K. Hydrogen atoms and disorder are omitted for clarity.

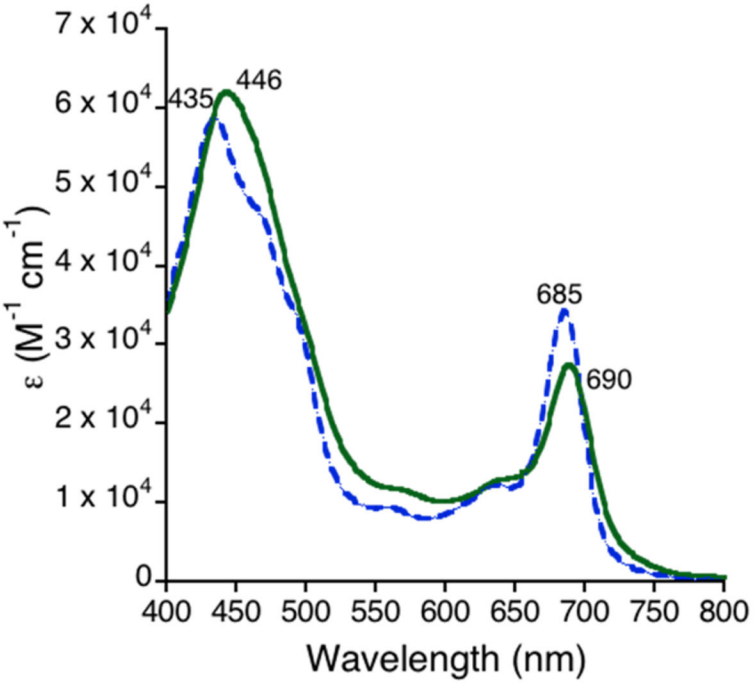

Figure 7.

UV–vis spectrum of $Mn^{III}(TBP_8Cz)$ (blue dashed line) and $Mn^{III}(MeOP_8Cz)$ (green solid line) in CH_2Cl_2.

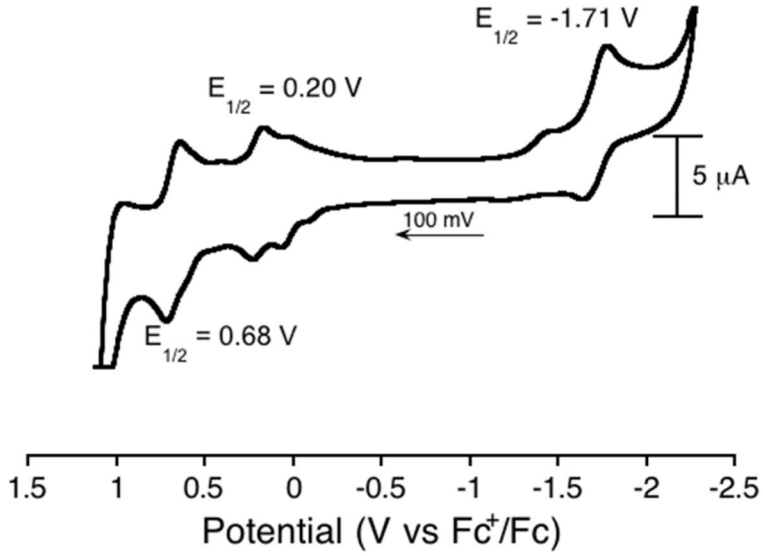

Figure 8.

Cyclic voltammogram for $Mn^{III}(MeOP_8Cz)$ (0.3 mM) in CH_2Cl_2 with 0.1 M $TBAPF_6$ electrolyte.

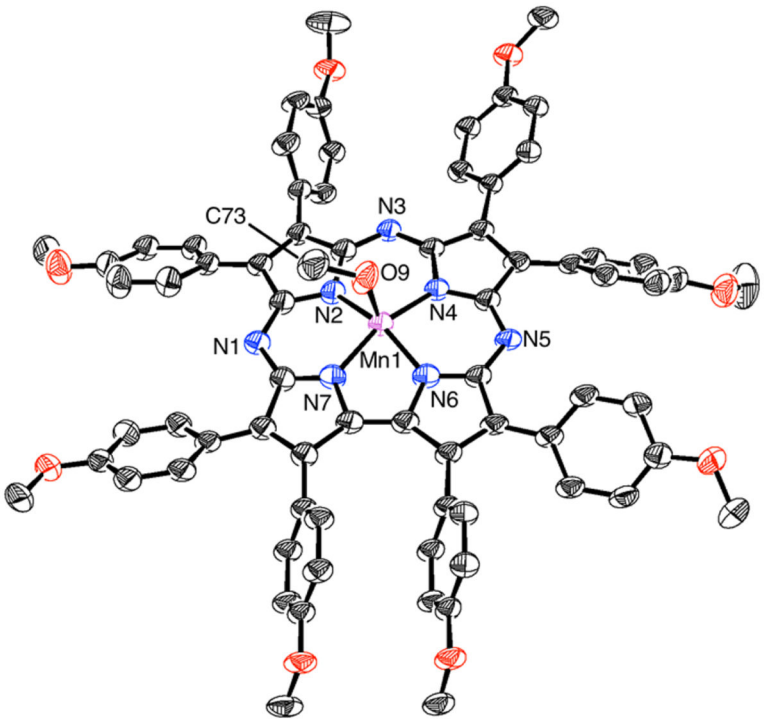

Figure 9.

Displacement ellipsoid plot (50% probability level) of $Mn^{III}(MeOP_8Cz)(MeOH)$ at 93(2) K. Hydrogen atoms and disorder are omitted for clarity.

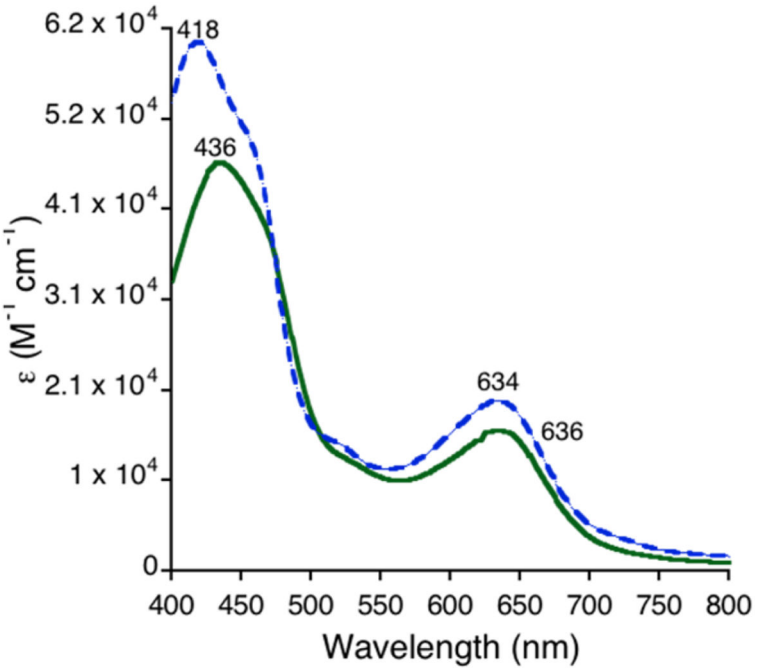

Figure 10.

UV–vis spectra of $Mn^{V}(O)(TBP_8Cz)$ (blue dashed line) and $Mn^{V}(O)(MeOP_8Cz)$ (green solid line) in CH_2Cl_2.

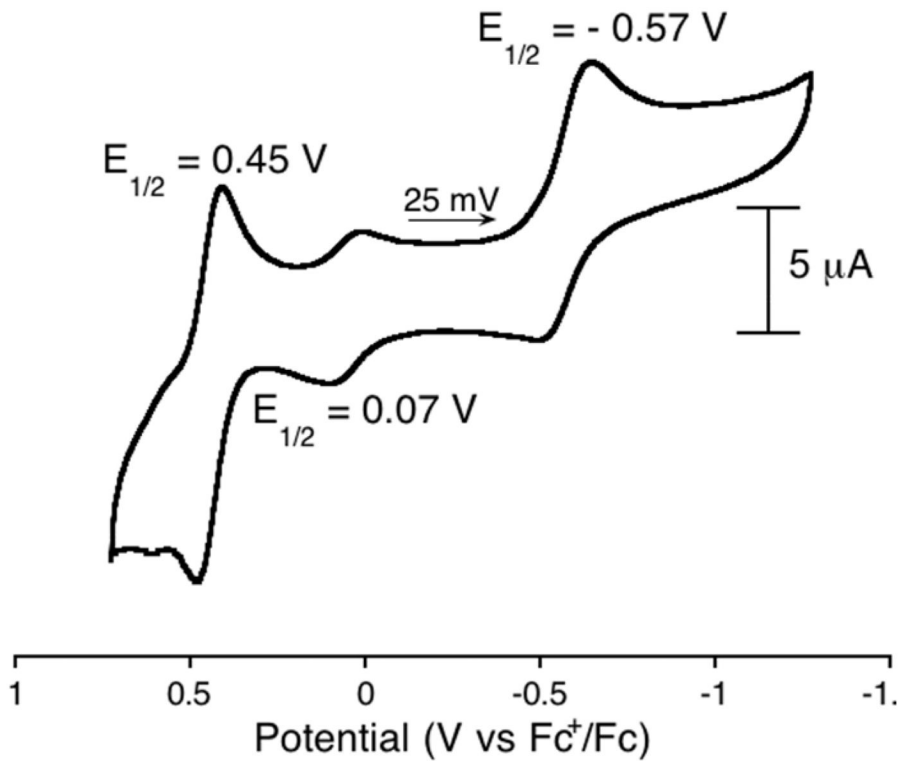

Figure 11.

Cyclic voltammogram for $Mn^{V}(O)(MeOP_8Cz)$ (0.3 mM) in CH_2Cl_2 with 0.1 M $TBAPF_6$ electrolyte.

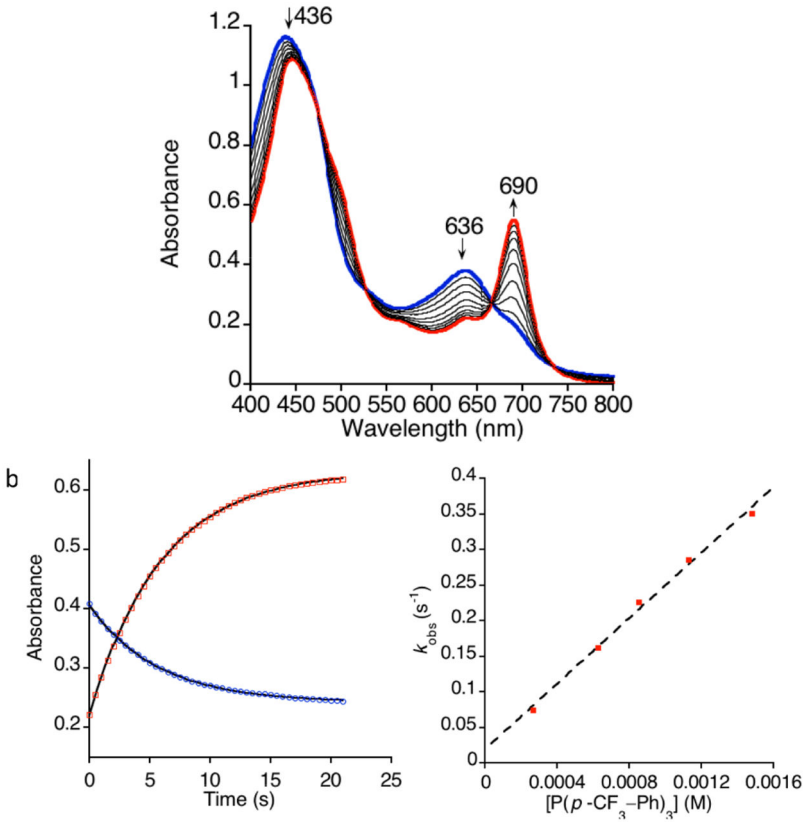

Figure 12.

(a) Time-resolved UV–vis spectral changes observed in the reaction of $Mn^{V}(O)(MeOP_8Cz)$ (26 μM) with P(*p*-CF_3–Ph)$_3$ (0.63 mM) in CH_2Cl_2 at 25 °C. (b) Changes in absorbance vs time for the growth of $Mn^{III}(MeOP_8Cz)$ (red ●) and decay of $Mn^{V}(O)$-$(MeOP_8Cz)$ (blue ■) with the best fit lines (black). (c) Plot of pseudo-first-order rate constants (k_{obs}) vs [P(*p*-CF_3–Ph)$_3$] (R^2 = 0.99).

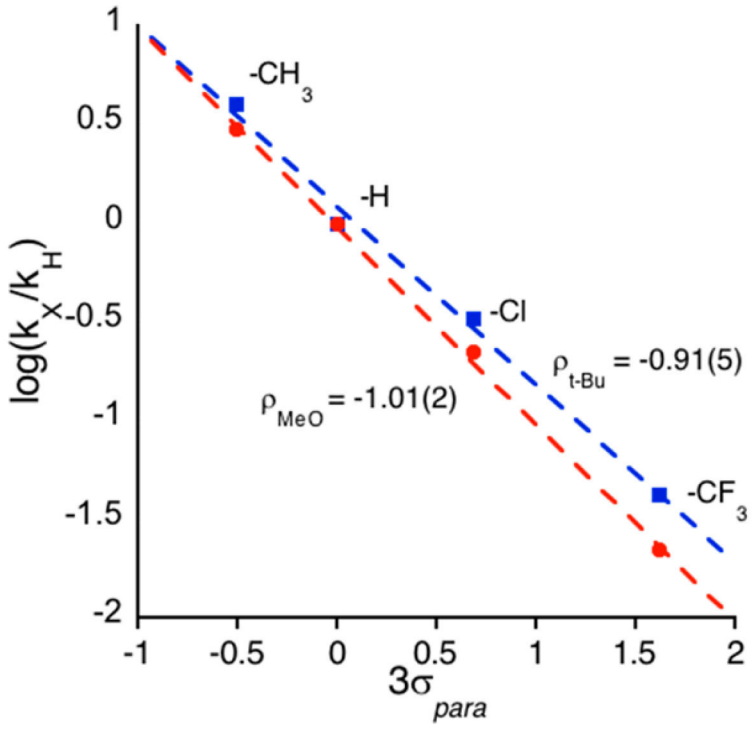

Figure 13.

Hammett plot for OAT reactions between PAr_3 and $Mn^{V}(O)(MeOP_8Cz)$ (red line) and $Mn^{V}(O)(TBP_8Cz)$ (blue line) in CH_2Cl_2 at 25 °C.

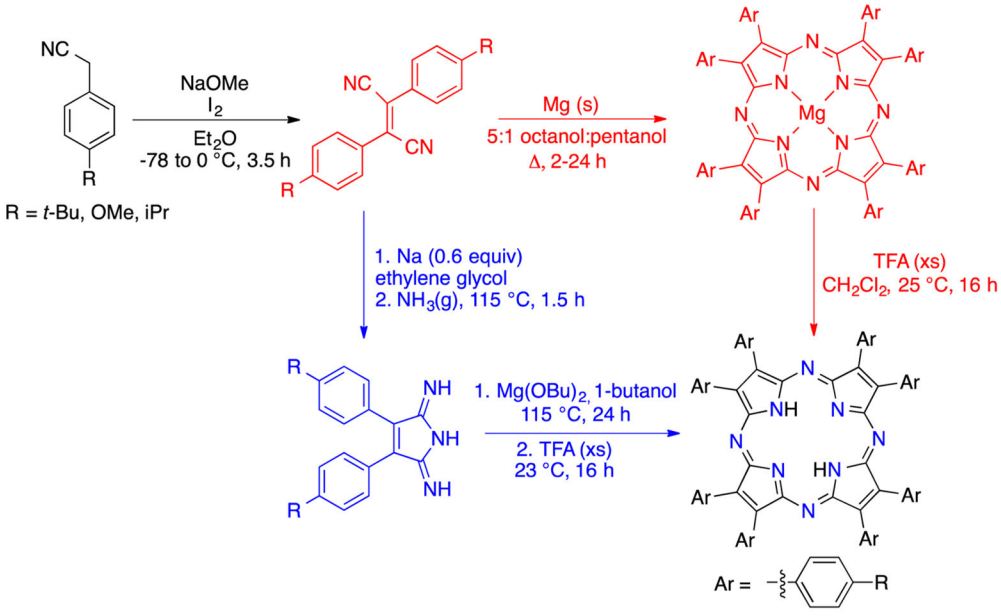

Scheme 1.

Synthetic Routes for the RP_8PzH_2

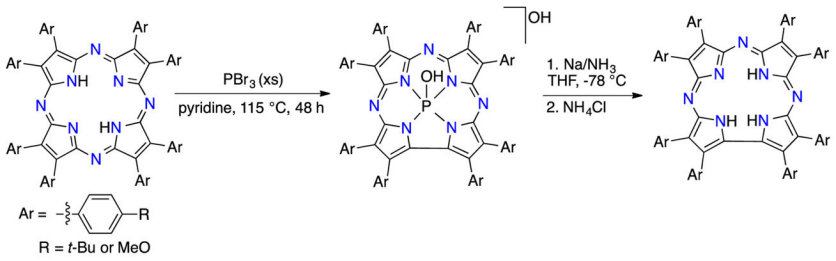

Scheme 2.
General Synthesis of RP_8CzH_3

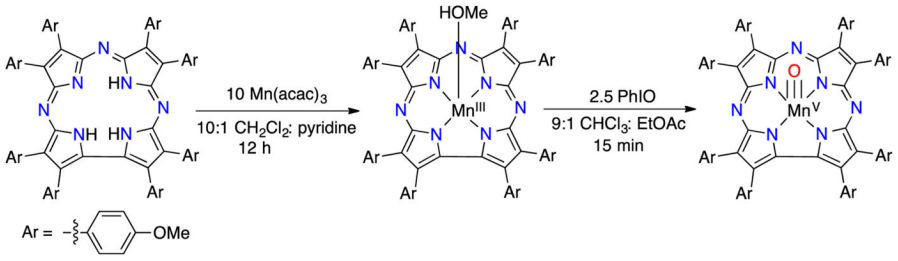

Scheme 3.
Synthesis of $Mn^{V}(O)(MeOP_8Cz)$

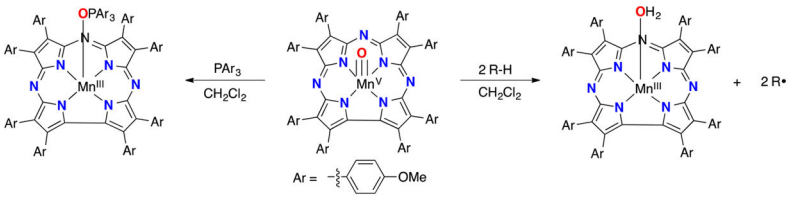

Scheme 4.

Hydrogen Atom Transfer (Right) And Oxygen Atom Transfer (Left) Of $Mn^{V}(O)(MeOP_{8}Cz)$ with Substrate

Table 1

Selected Bond Lengths (Å) and Bond Angles (deg) for $P^V(MeOP_8Cz)(OMe)_2$ and $P^V(TBP_8Cz)(OMe)_2$.[1]

	$P^V(MeOP_8Cz)(OMe)_2$	$P^V(TBP_8Cz)(OMe)_2$
P1–N2	1.7903(19)	1.75(2)
P1–N4	1.788(2)	1.82(2)
P1–N6	1.7761(19)	1.75(2)
P1–N7	1.777(2)	1.77(2)
P1–$(N_{pyrrole})_{plane}$	0.012	0.034
P1–$(23\text{-atom})_{core}$	0.051	0.065
Cα–Cα	1.423(3)	1.42(2)
P1–O9	1.6996(19)	1.69(1)
P1–O10	1.6792(19)	1.72(2)
O9–P1–O10	174.71(9	175.7(8)
N2–P1–N4	95.39(9)	93.5(7)
N4–P1–N6	90.73(9)	91.8(9)
N6–P1–N7	83.23(9)	82.8(8)
N7–P1–N2	90.64(9)	91.9(9)
N2–P1–O9	90.07(9)	85.6(8)
N4–P1–O9	85.32(9)	89.6(8)
N6–P1–O9	89.76(9)	94.6(8)
N7–P1–O9	93.79(9)	91.9(9)
N2–P1–O10	86.26(9)	91.4(8)
N4–P1–O10	91.21(9)	87.5(8)
N6–P1–O10	94.29(9)	88.6(8)
N7–P1–O10	90.07(9)	91.3(8)

Table 2

Selected Bond Lengths (Å) and Bond Angles (deg) for $Mn^{III}(MeOP_8Cz)(MeOH)$ and $Mn^{III}(TBP_8Cz)(MeOH)\cdot MeOH$[47]

	$Mn^{III}(MeOP_8Cz)(MeOH)$	$Mn^{III}(TBP_8Cz)(MeOH)$
Mn–N2	1.890(3)	1.892(4)
Mn–N4	1.887(3)	1.876(3)
Mn–N6	1.887(3)	1.885(3)
Mn–N7	1.886(3)	1.884(3)
$Mn–(N_{pyrrole})_{plane}$	0.337	0.373(2)
$Mn–(23\text{-atom})_{core}$	0.477	0.582(1)
$C\alpha–C\alpha$	1.394(5)	1.445(6)
Mn–O	2.130(5)	2.107(3)
N2–Mn–N4	94.16(12)	92.76(15)
N4–Mn–N6	89.25(13)	88.58(14)
N6–Mn–N7	80.45(13)	80.59(14)
N7–Mn–N2	88.80(13)	89.10(14)
N2–Mn–O9	96.6(2)	96.92(14)
N4–Mn–O9	102.0(2)	100.92(14)
N6–Mn–O9	104.5(2)	106.45(14)
N7–Mn–O9	107.0(5)	101.83(14)

Table 3

Spectroscopic UV–vis Comparison of *para*-Substituted Corrolazines

complex	Soret band λ_{max} (nm) ($\varepsilon \times 10^{-4}$ M^{-1} cm^{-1})	Q-band λ_{max} (nm) ($\varepsilon \times 10^{-4}$ M^{-1} cm^{-1})
$[P^{V}(MeOP_8Cz)(OH)]OH$	461 (8.2)	644 (4.5)
$[P^{V}(TBP_8Cz)(OH)]OH$	451 (13.7)	641 (8.0)
$\Delta_{MeO\text{-}tBu}$	10 nm	3 nm
$Mn^{III}(MeOP_8Cz)$	446 (5.50)	690 (2.48)
$Mn^{III}(TBP_8Cz)$	435 (5.85)	685 (3.49)
$\Delta_{MeO\text{-}tBu}$	11 nm	5 nm
$Mn^{V}(O)(MeOP_8Cz)$	436(4.53)	636 (1.54)
$Mn^{V}(O)(TBP_8Cz)$	418 (6.29)	634 (1.99)
$\Delta_{MeO\text{-}tBu}$	18 nm	2 nm

Table 4

Comparison of Rate Constants for HAT by Mn^{V}(O) Corrolazines

substrate	Mn^{V}(O)($MeOP_8Cz$) k (M^{-1} s^{-1})	Mn^{V}(O)(TBP_8Cz) k (M^{-1} s^{-1})	ratio k_{MeO}/k_{TBP}	BDFE (kcal mol^{-1})
1,4-cyclohexadiene[a]	$6.8(4) \times 10^{-5}$	$3.3(1) \times 10^{-5}$	2	76[b]
xanthene	$2.3(1) \times 10^{-3}$	$1.8(2) \times 10^{-3}$	1.3	74[c]
$AcrH_2$	$1.70(2) \times 10^{-1}$	$1.66(1) \times 10^{-1}$	1.0	69[c]

[a] Reference 26.

[b] BDE reported in the gas phase in ref 79.

[c] BDFE values reported in DMSO in ref 79. Rate constants normalized per reactive C–H bond n (e.g., $n = 2$ for xanthene).

Table 5

Second-Order Rate Constants for the Oxidation of Triarylphosphines by $Mn^{V}(O)$ Corrolazine

substrate	$Mn^{V}(O)(MeOP_8Cz)$ (M^{-1} s^{-1})	$Mn^{V}(O)(TBP_8Cz)$[a] (M^{-1} s^{-1})	ratio k_{TBP}/k_{MeO}
P(*o*-CH_3-Ph)$_3$	$1.02(5) \times 10^{1}$	$1.6(1) \times 10^{1}$	1.6
P(*p*-CH_3-Ph)$_3$	$3.1(2) \times 10^{4}$	$5.8(2) \times 10^{4}$	1.9
P(*p*-H-Ph)$_3$	$1.04(6) \times 10^{4}$	$1.43(6) \times 10^{4}$	1.3
P(*p*-Cl-Ph)$_3$	$2.3(1) \times 10^{3}$	$4.7(4) \times 10^{3}$	2.0
P(*p*-CF_3-Ph)$_3$	$2.3(1) \times 10^{2}$	$6.0(6) \times 10^{2}$	2.6

[a] Reference 83.